

 Open access • Journal Article • DOI:10.1002/GLIA.23587

## **Lipopolysaccharide-induced alteration of mitochondrial morphology induces a metabolic shift in microglia modulating the inflammatory response in vitro and in vivo** — [Source link](#)

[Syam Nair](#), [Kristina Sobotka](#), [Pooja Joshi](#), [Pierre Gressens](#) ...+8 more authors

**Institutions:** [University of Gothenburg](#), [Paris Diderot University](#), [St Thomas' Hospital](#), [RMIT University](#)

**Published on:** 01 Jun 2019 - [Glia](#) (Glia)

**Topics:** [Mitochondrial fission](#), [Mitochondrion](#), [Neuroinflammation](#), [Oxidative phosphorylation](#) and [Microglia](#)

Related papers:

- [Microglial M1/M2 polarization and metabolic states.](#)
- [Glucose pathways adaptation supports acquisition of activated microglia phenotype.](#)
- [Network integration of parallel metabolic and transcriptional data reveals metabolic modules that regulate macrophage polarization.](#)
- [Metabolic reprogramming in macrophages and dendritic cells in innate immunity](#)
- [A Breakdown in Metabolic Reprogramming Causes Microglia Dysfunction in Alzheimer's Disease.](#)

Share this paper:    

View more about this paper here: <https://typeset.io/papers/lipopolysaccharide-induced-alteration-of-mitochondrial-dfx2uz4wqx>



## King's Research Portal

DOI:

[10.1002/glia.23587](https://doi.org/10.1002/glia.23587)

*Document Version*

Peer reviewed version

[Link to publication record in King's Research Portal](#)

*Citation for published version (APA):*

Nair, S., Sobotka, K. S., Joshi, P., Gressens, P., Fleiss, B., Thornton, C., Mallard, C., & Hagberg, H. (2019). Lipopolysaccharide-induced alteration of mitochondrial morphology induces a metabolic shift in microglia modulating the inflammatory response in vitro and in vivo. *Glia*, *67*(6), 1047-1061. <https://doi.org/10.1002/glia.23587>

### **Citing this paper**

Please note that where the full-text provided on King's Research Portal is the Author Accepted Manuscript or Post-Print version this may differ from the final Published version. If citing, it is advised that you check and use the publisher's definitive version for pagination, volume/issue, and date of publication details. And where the final published version is provided on the Research Portal, if citing you are again advised to check the publisher's website for any subsequent corrections.

### **General rights**

Copyright and moral rights for the publications made accessible in the Research Portal are retained by the authors and/or other copyright owners and it is a condition of accessing publications that users recognize and abide by the legal requirements associated with these rights.

- Users may download and print one copy of any publication from the Research Portal for the purpose of private study or research.
- You may not further distribute the material or use it for any profit-making activity or commercial gain
- You may freely distribute the URL identifying the publication in the Research Portal

### **Take down policy**

If you believe that this document breaches copyright please contact [librarypure@kcl.ac.uk](mailto:librarypure@kcl.ac.uk) providing details, and we will remove access to the work immediately and investigate your claim.



**Lipopolysaccharide-induced alteration of mitochondrial morphology induces a metabolic shift in microglia modulating the inflammatory response *in vitro* and *in vivo***

Journal:	GLIA
Manuscript ID	GLIA-00368-2018.R1
Wiley - Manuscript type:	Original Research Article
Date Submitted by the Author:	n/a
Complete List of Authors:	Nair, Syam; Goteborgs Universitet Sobotka, Kristina; Goteborgs Universitet Joshi, Pooja; Université Paris Diderot gressens, Pierre; Université Paris Diderot; King's College London Flaiss, Bobbi; RMIT; King's College London; Université Paris Diderot Thornton, Claire; King's College London Mallard, Carina; Goteborgs Universitet Hagberg, Henrik; Goteborgs Universitet; King's College London
Key Words:	mitochondria, microglia, inflammation, metabolism, mitochondrial fission

SCHOLARONE™  
Manuscripts

1 Lipopolysaccharide-induced alteration of mitochondrial morphology induces a metabolic  
2 shift in microglia modulating the inflammatory response *in vitro* and *in vivo*

3

4 Syam Nair<sup>1,2</sup> , Kristina S. Sobotka<sup>1,2</sup>, Pooja Joshi<sup>3</sup>, Pierre Gressens<sup>3,4</sup>, Bobbi Fleiss<sup>3-5</sup>,  
5 Claire Thornton<sup>4</sup>, Carina Mallard<sup>1,2</sup>, Henrik Hagberg<sup>1,4,6</sup>

6

7 <sup>1</sup>Centre of Perinatal Medicine and Health, The Sahlgrenska Academy, University of  
8 Gothenburg, Gothenburg, Sweden;

9 <sup>2</sup>Institute of Neuroscience and Physiology, The Sahlgrenska Academy, University of  
10 Gothenburg, Gothenburg, Sweden;

11 <sup>3</sup>PROTECT, INSERM, Université Paris Diderot, Sorbonne Paris Cité, F-75019 Paris,  
12 France.

13 <sup>4</sup> Centre for the Developing Brain, Department of Division of Imaging Sciences and  
14 Biomedical Engineering, King's College London, King's Health Partners, St. Thomas'  
15 Hospital, London, SE1 7EH, United Kingdom;

16 <sup>5</sup>School of Health and Biomedical Sciences, RMIT University, Bundoora, VIC, Australia;

17 <sup>6</sup>Institute of Clinical Sciences, The Sahlgrenska Academy, University of Gothenburg,  
18 Gothenburg, Sweden.

19 **Running title:** LPS induced morphological and metabolic changes in microglia cells.

## 20 **Acknowledgements.**

21 We gratefully acknowledge the support from ERA-net (EU;VR 529-2014-7551), Wellcome  
22 Trust (WT094823), the Medical Research Council, Swedish Medical Research Council  
23 (VR 2015-02493, HH; VR 2012-2992, CM), Brain Foundation (HH, CM), Ahlen  
24 Foundation (HH, CM, SN), ALF-GBG (426401, HH; 432291, CM), and the Leducq  
25 Foundation (DSRRP34404), Torsten Söderberg (M98/15, CM), Frimurare  
26 Barnhusdirektionen (SN), to enable this study to be completed. In addition, the authors  
27 acknowledge financial support from the Department of Health via the National Institute  
28 for Health Research (NIHR) comprehensive Biomedical Research Centre Award to Guy's  
29 & St Thomas' NHS Foundation Trust in partnership with King's College London and King's  
30 College Hospital NHS Foundation Trust. Centre for Cellular Imaging at the University of  
31 Gothenburg and the National Microscopy Infrastructure, NMI (VR-RFI 2016-00968) for  
32 providing assistance in microscopy.

33

## 34 **Corresponding author:**

35 Henrik Hagberg, Department of Obstetrics and Gynecology,  
36 Institute of Clinical Sciences, Journalvägen 6, 41685 Göteborg,  
37 Email: [henrik.hagberg@gu.se](mailto:henrik.hagberg@gu.se)

38 Number of pages: 26, Number of figures: 9.

39

## 40 **Word count**

41 Abstract: 182, Introduction: 732, Materials and methods : 2331, Results:1405,  
42 Discussion: 1507, Total word count: 6205

43

44 **Conflict of interest:** We report no conflict of interest

**45 Abstract**

46 Accumulating evidence suggests that changes in the metabolic signature of microglia  
47 underlie their response to inflammation. We sought to increase our knowledge of how  
48 pro-inflammatory stimuli induce metabolic changes. Primary microglia exposed to LPS  
49 expressed excessive fission leading to more fragmented mitochondria than tubular  
50 mitochondria. LPS mediated TLR4 activation also resulted in metabolic reprogramming  
51 from oxidative phosphorylation to glycolysis. Blockade of mitochondrial fission by Mdivi-  
52 1, a putative mitochondrial division inhibitor led to the reversal of the metabolic shift. Mdivi-  
53 1 treatment also normalized the changes caused by LPS exposure, namely an increase  
54 in mitochondrial ROS production and mitochondrial membrane potential as well as  
55 accumulation of key metabolic intermediate of TCA cycle succinate. Moreover, Mdivi-1  
56 treatment substantially reduced LPS induced cytokine and chemokine production. Finally,  
57 we showed that Mdivi-1 treatment attenuated expression of genes related to cytotoxic,  
58 repair and immunomodulatory microglia phenotypes in an in vivo neuroinflammation  
59 paradigm. Collectively, our data show that the activation of microglia to a classically pro-  
60 inflammatory state associated with a switch to glycolysis that is mediated by mitochondrial  
61 fission, a process which may be a pharmacological target for immunomodulation.

62 **Key words:** inflammation, mitochondria, microglia, metabolism, mitochondrial fission

63 **Main points:**

64 LPS induces mitochondrial fragmentation and a metabolic switch in microglia.  
65 Blockade of fragmentation by Mdivi-1 reverses the metabolic shift, enhanced cytokine  
66 production, succinate accumulation *in vitro* and microglial activation *in vivo*.

## 67 **Introduction**

68 Microglia contribute to normal brain development, homeostasis and respond to  
69 pathological conditions by changing their phenotype from surveillance to pro-  
70 inflammatory, repair, regenerative and immunomodulatory states (Greter, Lelios, &  
71 Croxford, 2015; Tay, Savage, Hui, Bisht, & Tremblay, 2017). Studies of adult and  
72 neonatal injury and disease have conclusively shown that changes in the phenotype of  
73 microglia play a role in almost all forms of neuropathology (Solito & Sastre, 2012).  
74 Transcriptome analysis of microglia exposed to inflammatory stimuli revealed transient  
75 upregulation of important and stimulus-specific metabolic pathways (Thion et al., 2018),  
76 strongly suggesting that energy metabolism is modulated during brain inflammation.  
77 Microglia activation in response to stimuli that includes pathogen associated proteins,  
78 such as lipopolysaccharide (LPS), is a metabolically energy expensive event (Moss &  
79 Bates, 2001).

80 Mitochondria, which play a central role in energy metabolism, are dynamic organelles that  
81 undergo biogenesis, fission, fusion and mitophagy (autophagic degradation). The  
82 balance of these processes allows the reorganization of mitochondrial components and  
83 the elimination of damaged material, thereby maintaining a healthy mitochondrial  
84 population (Pickles, Vigie, & Youle, 2018; Wai & Langer, 2016) . Recent studies have  
85 linked mitochondrial dynamics to energy demand, suggesting changes in mitochondrial  
86 architecture as a mechanism for bioenergetic adaptation to inflammation (Nasrallah &



87 Horvath, 2014). By favoring either elongated or fragmented structures, mitochondria can  
88 regulate bioenergetic ability and thereby cell fate through metabolic programming (Buck  
89 et al., 2016). Although mitochondrial morphological changes are observed in response to  
90 alterations in oxidative metabolism (Hackenbrock, 1966), little is known of its role in  
91 microglia activation.

92 Microglia generate energy via both oxidative phosphorylation (OXPHOS) and glycolysis  
93 (Orihuela, McPherson, & Harry, 2016). OXPHOS occurs within the mitochondria and is  
94 more efficient for ATP synthesis in comparison to glycolysis. However, the preferential  
95 use of glycolysis over OXPHOS for ATP production enables activated microglia to  
96 produce ATP at a faster rate (Schuster, Boley, Moller, Stark, & Kaleta, 2015). Enhanced  
97 glycolysis supplies biosynthetic intermediates for cell growth and rapid production  
98 intermediates for cytokine production such as reactive oxygen species (ROS) thereby  
99 enabling effector functions (Chang et al., 2013; Everts et al., 2014). In macrophages or  
100 dendritic cells, pro-inflammatory stimuli cause them to undergo a metabolic switch from  
101 OXPHOS to glycolysis, a phenomenon similar to the Warburg effect (Kelly & O'Neill,  
102 2015). Microglia share many functions and characteristics with macrophages (Butovsky  
103 & Weiner, 2018) but they are from a distinct non-hematopoietic lineage, and whether a  
104 similar switch from OXPHOS to glycolysis has not been explored in microglia.

105 We have previously found that both Toll-like receptor (TLR)-induced inflammation and  
106 mitochondrial dysfunction are involved in the development of neonatal brain injury

107 (Hagberg, Mallard, Rousset, & Thornton, 2014; Mottahedin et al., 2017). We have also  
108 found that mitochondrial ROS production and inflammation is increased after neonatal  
109 brain injury associated with altered Krebs cycle and succinate accumulation in the  
110 mitochondria (Koning et al., 2017). Activation of microglia results in an altered Krebs  
111 cycle, as a result of metabolic switch promoting inflammatory gene expression (Gimeno-  
112 Bayon, Lopez-Lopez, Rodriguez, & Mahy, 2014; Leaw et al., 2017; Orihuela et al., 2016).  
113 Katoh et al. found that that mitochondrial fission via the activation of DRP1 (by TLR4  
114 stimulation) increases mitochondrial fission but they did not look in to metabolism or  
115 cytokine production in microglia (Katoh et al., 2017). Here, we add data on how TLR4  
116 activation affects mitochondrial morphology, energy metabolism, ROS and cytokine  
117 production in microglia. This knowledge is important given the many roles of microglia in  
118 mediating host-defenses, and how these processes can mediate injury to the brain when  
119 activation is aberrant and prolonged. ROS signaling has been demonstrated to result in  
120 damage to cell components; at the same time ROS production is essential for host  
121 defenses (Y. Zhang et al., 2012).

122 In this study, we investigated the link between mitochondrial architecture and metabolic  
123 reprogramming in primary microglia after induction to a prototypical pro-inflammatory  
124 activation state via LPS-mediated TLR4 activation. We also used the putative  
125 mitochondrial fission inhibitor, Mdivi-1 (Cassidy-Stone et al., 2008) to modulate  
126 mitochondrial dynamics *in vitro* and *in vivo*. We found that pro-inflammatory activation of

127 microglia changes the mitochondrial dynamics including a metabolic switch from  
128 OXPHOS to glycolysis and that Mdivi-1 reverses these effects and the expected LPS-  
129 induced cytokine production and ROS production *in vitro*. Further, we investigated the  
130 effect of Mdivi-1 in an *in vivo* paradigm of neuroinflammation and found that Mdivi-1  
131 reduced the expression of genes related to cytotoxic, repair and immunomodulatory  
132 microglia phenotypes.

### 133 **Materials and Methods**

#### 134 ***Animals of in vitro* experiments**

135 Pregnant C57BL/6 mice were sourced from Charles River Laboratories International  
136 (Sulzfeld, Germany). C57BL/6J-Tg(CAG-Cox8/EGFP)49Rin mice (Cox8/EGFP;  
137 RBRC02250) expressing endogenous green fluorescent protein in cytochrome c oxidase,  
138 subunit VIIIa of mitochondria (Shitara et al., 2001) were obtained from Riken bio resource  
139 center, Japan. Animals were housed and bred at the Experimental Biomedicine animal  
140 facility (University of Gothenburg, Gothenburg, Sweden) under specific pathogen free  
141 conditions on a 12 h light/dark 7 cycle with *ad libitum* access to standard laboratory chow  
142 (B&K, Solna, Sweden) and water. All experiments were approved by the local ethical  
143 committee at University of Gothenburg (No: 203-2014 and 32-2016) and performed  
144 according to the Guidelines for the care and use of Laboratory Animals.

**145 Microglial cell culture**

146 Primary cultures of purified microglia were created from 1 to 3-day-old C57BL/6 or  
147 Cox8/EGFP mice of both sexes, as previously described (Dean et al., 2010) with minor  
148 adaptations. Following decapitation, the brain was isolated with the meninges removed  
149 and washed in ice-cold Hanks buffered salt solution (HBSS; Sigma–Aldrich, St Louis, MO,  
150 USA) supplemented with 100 U/mL penicillin and 100 µg/mL streptomycin (Sigma–  
151 Aldrich). Forebrains were dissociated by gentle trituration in Dulbecco’s modified Eagle’s  
152 medium (DMEM; Sigma–Aldrich) supplemented with 20% heat-inactivated fetal bovine  
153 serum (FBS; Fischer Scientific, Goteborg, Sweden) and antibiotics. The cell suspension  
154 was passed through a 70 µm cell sieve (Falcon, Corning, USA), plated in 75-cm<sup>2</sup> flasks  
155 with vented caps (Sarstedt, Germany) at a density of two brains/flask, and cultured  
156 undisturbed for seven days with HBSS/20% FBS/antibiotics. Medium was then replaced  
157 with HBSS/10% FBS/antibiotics, and cells were cultured for a further seven days.  
158 Microglia were selectively detached from the flasks by shaking (3 h, 37°C, 250 rpm) on a  
159 rotary shaker and the microglia cell suspension was collected and centrifuged (250 g ×  
160 10 min). The media were then removed, the pellet was suspended in DMEM/2%  
161 FBS/antibiotics and the number of cells were counted with an automated cell counter  
162 (Scepter; Millipore) and seeded into Seahorse XFe96 or 24 cell well plates (1× 10<sup>5</sup> cells  
163 per well). The purity of microglia cells was evaluated by immunocytochemical staining  
164 using antibodies against ionized calcium binding adapter molecule 1 (Iba1; 1:1000; Wako  
165 Pure Chemical Industries, Ltd., Richmond, VA, USA) and DAPI (1:1000; Sigma–Aldrich),

166 and was routinely greater than 99%. All incubations were performed at 37° C in a  
167 humidified atmosphere containing 5% CO<sub>2</sub> and 95% air.

### 168 **Sample Preparation for microscopy**

169 Primary microglia cells cultured from Cox8/EGFP mice were used for mitochondrial  
170 morphology analysis. Microglia cells were washed with PBS and plated on precision cover  
171 glasses thickness No. 1.5H (tol.  $\pm$  5  $\mu$ m) in a 24-well plate, with  $1 \times 10^5$  cells per well, and  
172 left to adhere overnight at 37°C in a cell culture incubator. Cells were fixed with 4%  
173 paraformaldehyde in culture media for 10 min and then mounted in ProLong Diamond  
174 antifade reagent (Life Technologies, Grand Island, NY) according to the manufacturer's  
175 instructions.

### 176 **Live cell imaging**

177 Primary microglia cells were seeded on MatTek (MatTek , Ashland, MA) glass bottom  
178 culture dishes. Following cell adherence, cells were exposed to DMSO alone (control) or  
179 LPS 100ng/ml for 24h or cells were pre-treated with Mdivi-1 (25  $\mu$ M; Sigma, St. Louis,  
180 MO, USA) for 1h followed by LPS (100ng/ml) exposure for 24hrs. Cells were washed  
181 gently three times with warm PBS. Further anti-bleaching live cell visualization medium  
182 (DMEMgfp-2, Evrogen) was added to the cells 30 min before imaging. Images were  
183 acquired with a Zeiss LSM 880 Airyscan super-resolution system with live cell capabilities  
184 and fitted with a fast-ASmodule (Carl Zeiss, Oberkochen, Germany). Microscopes were

185 equipped with an environmental chamber that maintained 37°C with humidified 5% CO<sub>2</sub>  
186 gas during imaging.

### 187 **Super-Resolution Structured illumination microscopy (SR-SIM)**

188 Super-resolution structured illumination microscopy (SR-SIM) on a Zeiss ELYRA PS.1  
189 microscope (Carl Zeiss Microscopy, Germany) was used to yield a 2-fold improvement in  
190 all spatial directions (Huang, Bates, & Zhuang, 2009) beyond the classical Abbe-Rayleigh  
191 limit. GFP was imaged using a Plan-Apochromat 100×/1.4 oil objective, an excitation  
192 wavelength of 488 nm and an emission wavelength range of 495-575 nm. The SR-SIM  
193 images were acquired as z-stacks with three angles and five phases in each plane and  
194 the z-step between planes was 3.30 nm. SR-SIM processing was performed using the  
195 Zeiss Zen software package. 3D rendering was done using Volocity 6 (Perkin-Elmer) and  
196 figures were compiled using Photoshop CC software (Adobe Systems, San Jose, CA).

### 197 **Mitochondrial morphology analysis**

198 Primary microglia were treated with LPS, Mdivi-1 or DMSO as described previously and  
199 mitochondria were categorised based on length: fragmented (<1 µm), tubular (1–3 µm)  
200 and elongated (>3 µm), as described previously (Jahani-Asl et al., 2011). Over 20 cells  
201 were analysed in Control, LPS-treated, LPS plus Mdivi-1 in three independent  
202 experiments. Volocity 6 was used for 3D rendering and to quantify mitochondrial length,  
203 volume and number.

204 **Measurement of Oxygen Consumption Rate (OCR) and Extracellular Acidification Rate**  
205 **(ECAR)**

206 Real-time measurements of oxygen consumption rates, and extracellular acidification  
207 rates, a measure of lactate production, were performed on an XFe96 Seahorse  
208 extracellular flux analyser (Seahorse Biosciences, North Billerica, MA). The optimal  
209 seeding density and test compound concentrations were empirically determined prior to  
210 initiation of experiments. According to the methods described in the XFe96 Extracellular  
211 Flux Analyzer User Manual (Seahorse Bioscience), preliminary studies were run with  
212 Carbonyl cyanide-4-(trifluoromethoxy)phenylhydrazone (FCCP) to identify the optimal  
213 number of cells required to observe a sufficient shift in OCR and ECAR. Once the cell  
214 number was decided, we determined the optimal working concentrations for each of the  
215 stimulating compounds used in the mitochondrial function analysis (oligomycin, FCCP,  
216 and rotenone). Cells were then plated into XFe96 cell culture plates (Seahorse  
217 Biosciences, North Billerica, MA) at a density of 10,000/well in 80  $\mu$ l of DMEM (Sigma–  
218 Aldrich, St Louis, MO, USA). Cells were allowed to adhere overnight in a 37°C incubator  
219 with 5% CO<sub>2</sub>. Following cell adherence, cells were exposed to a final concentration of  
220 Ultra-pure LPS 50 or 100ng/ml (*Escherichia coli* 055: B5, Biological Laboratories,  
221 Campbell, CA) or media alone (control) for 3, 6 or 24 h. For mitochondrial fission blocking  
222 experiments, microglia cells were pre-treated with Mdivi-1 (25  $\mu$ M) or DMSO for 1 h before  
223 LPS exposure. Media (80  $\mu$ L) was removed followed by the addition of 200  $\mu$ L XF base  
224 media (180  $\mu$ l) supplemented with 10mM glucose, 5mM pyruvate, and 2mM glutamine for

225 OCR. For ECAR only 2mM glutamine was added following incubation in a non-CO<sub>2</sub>  
226 chamber for 1 h.

227 The day prior to the experiment, 200µl of XF calibration media was added to the XF  
228 sensor cartridges and kept in a non-CO<sub>2</sub> incubator for 24h. XF sensor cartridges were  
229 loaded with test compounds and OCR/ECAR measured. OCR was measured by  
230 sequential injections of oligomycin (1µM final concentration, blocks ATP synthase to  
231 assess respiration required for ATP turnover), FCCP (carbonyl cyanide 4-  
232 trifluoromethoxy-phenylhydrazone, 2µM final concentration, a proton ionophore  
233 uncoupler inducing maximal respiration), and rotenone plus antimycin A (1µM final  
234 concentration of each, which completely inhibits electron transport to measure non-  
235 mitochondrial respiration).

236 ECAR was measured under glucose-starved microglia. Basal glycolysis rate was  
237 determined by injecting glucose at a final concentration of 10mM. For estimating glycolytic  
238 capacity, oligomycin was injected at a final concentration of 5µM. Finally, 2-deoxyglucose  
239 (2-DG) was injected at a final concentration of 50mM to measure the non-glycolytic  
240 acidification. Each step had three cycles; each cycle consisted of 3 min mixing, 2 min  
241 incubation and 3 min measurement. All experiments were run in three replicates with 3-4  
242 sample per replicates. Cell counts were used to normalize OCR and ECAR.



**243 Multiplex cytokine assay**

244 Bio-Plex Pro Mouse Cytokine Standard 23-Plex kit (Bio-Rad) was used to measure the  
245 concentrations of cytokines/chemokines in microglia-cultured media following the  
246 manufacturer's protocol. Microglia conditioned media was collected from microglia  
247 samples used in the OCR and ECAR experiments explained above. Samples were  
248 normalized to cell number ( $1 \times 10^5$ ; 1:10 in diluent buffer) and concentrations of IL-1 $\alpha$ , IL-  
249 1 $\beta$ , IL-2, IL-3, IL-4, IL-5, IL-6, IL-9, IL-10, IL-12 (p40), IL-12 (p70), IL-13, IL-17a, eotaxin,  
250 granulocyte colony-stimulating factor (G-CSF), granulocyte macrophage colony-  
251 stimulating factor (GM-CSF), interferon-gamma (IFN- $\gamma$ ), KC/chemokine (C-X-C motif)  
252 ligand 1 (CXCL1), monocyte chemotactic protein-1 (MCP-1)/chemokine (C-C motif)  
253 ligand 2 (CCL2), macrophage inflammatory protein 1 $\alpha$  (MIP-1 $\alpha$ )/CCL3, MIP-1 $\beta$ /CCL4,  
254 RANTES, and TNF- $\alpha$  were simultaneously quantified on a Bio Plex 200 System (Bio-Rad,  
255 Sweden) and data presented as Log<sub>10</sub> of cytokine concentrations (picograms per  
256 millilitre).

**257 Succinate level measurement**

258 Microglia cells were pre-treated with vehicle (DMSO), Mdivi-1 (25  $\mu$ M; Sigma, St. Louis,  
259 MO, USA) for 1h or dimethyl malonate (DMM; 10mM; Sigma, St. Louis, MO, USA) for 3h  
260 before stimulation with LPS (100 ng/ml) for 24 h. Succinate Colorimetric Assay Kit  
261 (Sigma-Aldrich Inc., St Louis, MO, USA) was used to determine the succinate  
262 concentrations according to the manufacturer's instructions. Microglia cells ( $1 \times 10^5$  cells

263 per well) were rapidly homogenized on ice in 100 $\mu$ L of ice-cold succinate assay buffer  
264 and centrifuged at 10,000 $\times$ g for 5 min to remove insoluble material. Then, cell  
265 homogenates were added into a 96-well plate in duplicate wells and mixed with reaction  
266 mix provided in with the kit, which results in a colorimetric product proportional to the  
267 succinate present. The resultant mixtures were further incubated at 37°C for 20 min. The  
268 succinate concentration was determined by the standard curve using spectroscopy at  
269 450nm wavelength.

#### 270 **Measurement of mitochondrial ROS production by live cell imaging.**

271 Mitochondrial superoxide generation was assessed in live cells using MitoSOX (Molecular  
272 Probes), a fluorogenic dye that is taken up by mitochondria, where it is readily oxidized  
273 by superoxide ( $O_2^{\cdot-}$ ). MitoSOX Red reagent is a novel fluorogenic dye specifically  
274 targeted to mitochondria in live cells. Oxidation of MitoSOX Red reagent produces red  
275 fluorescence by superoxide but not by other ROS or Reactive Nitrogen Species-  
276 generating systems. Primary microglia cells were seeded on MatTek (MatTek , Ashland,  
277 MA) glass bottom culture dishes ( $1 \times 10^5$  cells/dish) and left to adhere overnight. Following  
278 treatments described above, live microglia were incubated with 5 $\mu$ M MitoSOX at 37°C for  
279 10 min. Cells were washed gently three times with warm PBS further anti-bleaching live  
280 cell visualization medium (DMEMgfp<sup>-2</sup>) was added to the cells 30 min before imaging.  
281 Airyscan super-resolution microscopy on a LSM 880 (Carl Zeiss Microscopy, Germany)  
282 with an onboard incubator at 37°C was used to acquire images using a 63 $\times$  oil objective,

283 an excitation wavelength of 488nm. Airyscan-processing was done using the Zeiss Zen  
284 software package. MitoSox fluorescence was quantified using Volocity 6.

285 **Measurement of the mitochondrial membrane potential by live cell imaging.**

286 JC-1 (Molecular Probes) is a cationic dye that exhibits mitochondrial membrane potential-  
287 dependent accumulation in mitochondria, indicated by a fluorescence emission shift from  
288 green (~525 nm) to red (~590 nm). Mitochondrial depolarization is indicated by a  
289 decrease in the red to green fluorescence intensity ratio. The potential sensitive color shift  
290 is due to concentration dependent formation of red fluorescent aggregates. Primary  
291 microglia cells were seeded, incubated and treated as above. Following LPS exposure,  
292 the media was removed cells were incubated with JC-1 (2 $\mu$ M final concentration) and  
293 incubated at 37°C, 5% CO<sub>2</sub> for 20 min. Cells were washed gently three times with warm  
294 PBS and further anti-bleaching live cell visualization medium (DMEMgfp<sup>-2</sup>) was added to  
295 the cells 30 min before imaging. Images were scanned using an oil immersion, 63 $\times$ , and  
296 1.3 NA objective. Samples were excited at wavelength of 488nm and emission  
297 wavelength of 547 and 617 nm. The confocal pinhole aperture was set to 50, and the  
298 voltage to the photomultiplier tubes of each channel was maintained at equal values.  
299 Illumination was limited to periods of image acquisition. Images were exactly in phase  
300 and represented the amount of monomeric and J-aggregate JC-1 fluorescence.

301 **Effect of Mdivi-1 in an *in vivo* model of inflammation-mediated damage to the preterm**  
302 **brain**

303 We employed a well characterized paradigm of systemic inflammation driven  
304 neuroinflammation (Favrais et al., 2011; Krishnan et al., 2017; Van Steenwinckel et al.,  
305 2018), which is known to have effects on brain development and behavior consistent with  
306 those reported in infants and children born preterm (Ball et al., 2017; Raju, Buist, Blaisdell,  
307 Moxey-Mims, & Saigal, 2017) . Experimental protocols were approved by the institutional  
308 guidelines of the Institute National de la Santé et de la Recherche Scientifique (Inserm)  
309 France. The treatments was carried out as per previously described in full (Favrais et al.,  
310 2011), with a shortened protocol described below. Assessment of gene expression were  
311 made only in male animals as female animals are not injured in this paradigm, mimicking  
312 the male predisposition to injury observed in male preterm born infants (Peacock,  
313 Marston, Marlow, Calvert, & Greenough, 2012). Briefly, mice received twice a day from  
314 P1 to P2 and once on P3 a 5- $\mu$ l intra-peritoneal injection of 10  $\mu$ g/kg/injection recombinant  
315 mouse IL-1 $\beta$  in phosphate buffered saline (PBS; R&D Systems, Minneapolis, MN) or PBS  
316 alone or P1–P3 pups were co-injected with IL-1 $\beta$  and 3 mg/kg/injection of Mdivi-1 (IP,  
317 5ul).

318 **Isolation and ex vivo microglia and gene expression analysis**

319 At P3, brains were collected for cell dissociation and CD11B+ cell separation using a  
320 magnetic coupled antibody anti-CD11B (Miltenyi, MACS Technology) as previously

321 described in detail (Krishnan et al., 2017; Schang et al., 2014; Shiow et al., 2017).  
322 Microglia are the predominant CD11B cell in this model of injury by more than 100 fold  
323 compared to populations of either macrophage or neutrophil (Krishnan et al., 2017).  
324 Total RNA was extracted from the CD11B+ microglia cells with the RNeasy mini kit  
325 (Qiagen, France), RNA quality and concentration were assessed by spectrophotometry  
326 (Nanodrop™, ThermoFisher Scientific, MA, USA). Reverse transcription was achieved  
327 with the iScript™ cDNA synthesis kit (Bio-Rad, France) and RT-qPCR was performed in  
328 triplicate for each sample using SYBR Green Super-mix (Bio-Rad) as previously  
329 described (Chhor et al., 2013). Primers were designed using Primer3 plus software (See  
330 sequences in Sup. Table 1). Specific mRNA levels were calculated after normalization to  
331 Rpl13a mRNA (reference gene) based on previous reference gene suitability testing. The  
332 data are presented as relative mRNA units with respect to the control group (expressed  
333 as fold over control value).

### 334 **Statistics**

335 All statistics are reported as mean  $\pm$  SEM, performed using GraphPad Prism 7.0  
336 (GraphPad Software). Significance scores are \* for  $p < 0.05$ , \*\* for  $p < 0.01$ , \*\*\* for  $p <$   
337  $0.001$  and \*\*\*\*  $p < 0.0001$ .

338

## 339 **Results**

### 340 **LPS exposure induces excessive mitochondrial fragmentation in microglial cells.**

341 Mitochondrial morphology was examined in primary microglia cells cultured from Cox8-  
342 EGFP mice exposed to 50 or 100ng/mL LPS using 3D SR-SIM microscopy. The number  
343 of fragmented mitochondria was significantly increased in microglia cells stimulated with  
344 100ng/ml LPS for 24h (Fig 1c), and elongated and tubular mitochondria were decreased  
345 compared with untreated controls (Fig 1g). These findings are in line with previous studies  
346 in BV2 cells (Park et al., 2013) and primary microglia but with a higher dose of LPS  
347 (1ug/ml) (Kato et al., 2017). There was no change in the morphology of cells stimulated  
348 with 50ng/ml LPS for 24h (Fig 1b,g).

### 349 **LPS induces a switch from oxidative phosphorylation (OXPHOS) to glycolysis (metabolic 350 reprogramming) in microglia cells.**

351 Oxygen consumption rates (OCR) and extracellular acidification rates (ECAR) was  
352 measured in real time as measures of mitochondrial respiration and glycolysis for 50ng/ml  
353 LPS (fig 2a-c & i-k) and 100ng/LPS (Fig. 2o-q & w-y) respectively (Wu et al., 2007) with  
354 the Seahorse XFe96. Basal OCR and ATP-linked OCR was significantly increased in  
355 microglia cells following exposure to 50ng/ml LPS for 6-24h compared to controls (Fig.2d-  
356 e). FCCP-induced maximal OCR and spare respiratory capacity (SRC) decreased  
357 whereas leak-driven OCR significantly increased with exposure to 50ng/mL of LPS (Fig.  
358 2f-h). The ECAR parameters (glycolysis, glycolytic capacity and glycolytic reserve) were

359 increased following exposure to 50ng/ml LPS for 6-24hrs compared to controls (Fig. 2l-  
360 n). These results show that a moderate dose of LPS increases both OCR and glycolysis.  
361 Exposure to 100ng/mL of LPS for 6h resulted in an increase in basal OCR, ATP-linked  
362 OCR and leak-linked OCR compared to controls (Fig. 2r-s). In contrast, there was a  
363 significant decrease in basal OCR and ATP linked OCR at 24h after 100ng/mL LPS (Fig.  
364 2r,s,u). FCCP-induced maximal OCR and SRC significantly decreased at 24h 100ng/mL  
365 LPS (Fig. 2t-u). Glycolytic parameters increased with 100ng/ml LPS exposure for 3-24h  
366 compared with controls (Fig.2w-y). The overall decrease in OCR and increase in ECAR  
367 parameters with 100ng/ml LPS for 24h indicates a metabolic switch from OXPHOS to  
368 glycolysis.

### 369 **Mdivi-1 treatment blocks LPS-induced mitochondrial fragmentation and ROS production.**

370 Many conserved GTPase proteins are involved in mitochondrial fusion and fission  
371 dynamics such as mitofusins (MFN1 and MFN2) and dominant optic atrophy 1 (OPA1)  
372 are needed for the fusion of mitochondrial outer and inner membranes (Song, Ghochani,  
373 McCaffery, Frey, & Chan, 2009). Dynamin-related protein 1 (DRP1) and mitochondrial  
374 Fission 1 protein (FIS1) are the main mitochondrial fission mediators (Frezza et al., 2006).  
375 We used the mitochondrial fission inhibitor Mdivi-1 (Ruiz, Alberdi, & Matute, 2018) as the  
376 high (100 ng/ml) dose of LPS induced an increase in fragmented mitochondria (Fig. 3b).  
377 We examined the effect of pharmacologically blocking mitochondrial fission in LPS-  
378 exposed microglia cells cultured from Cox8/EGFP mice by pre-treatment with 25  $\mu$ M

379 Mdivi-1 for 1 h followed by incubation with LPS (100 ng/ml) for 24h. Results revealed that  
380 LPS-induced excessive mitochondrial fragmentation was significantly inhibited by Mdivi-  
381 1 pre-treatment and normalized mitochondrial morphology (Fig. 3c). Mdivi-1 treatment  
382 before LPS exposure reduced the number of fragmented mitochondria and increased the  
383 number of tubular and elongated mitochondria to control levels (Fig. 3d) .

384 **Mdivi-1 treatment normalized oxygen consumption and extracellular acidification rate in**  
385 **the microglia cells.**

386 Since Mdivi-1 restored mitochondrial morphology, we interrogated its effect on cellular  
387 respiration and ECAR-dependent glycolysis and glycolytic capacity (Fig. 4a, b, h, i).  
388 Mdivi-1 pre-treatment in cells exposed to LPS (100ng/ml for 6h) exhibited a decrease in  
389 the level of basal respiration and ATP-linked OCR to control levels compared to LPS  
390 treated cells (Fig. 4c-d). Conversely, Mdivi-1 treatment in cells exposed to 100ng LPS for  
391 24h led to an increase in basal and ATP-linked OCR compared to non-treated LPS  
392 exposed cells (Fig. 4c-d). Mdivi-1 treatment also increased FCCP-induced maximal OCR  
393 at 24h and leak-driven OCR compared to LPS exposed cells at both time points (Fig. 4e-  
394 f). Administration of Mdivi-1 in combination with LPS normalized the spare respiratory  
395 capacity (Fig. 4g). ECAR measurements showed that glycolysis and glycolytic capacity  
396 was significantly reduced to control levels in Mdivi-1 treated cells at 6 and 24h 100ng/ml  
397 LPS exposure (Fig.4h-k) compared to LPS exposed cells.



398 **Mdivi-1 reduces the LPS induced release of cytokines and chemokines.**

399 To show how LPS activation was inducing an inflammatory reaction in the primary  
400 microglia and to test whether this was effected by Mdivi-1 we measured cytokine and  
401 chemokine response in microglia conditioned media after treatment with of LPS and or  
402 Mdivi-1 (supporting information Fig. S1 and S2). As expected both doses, of LPS led to  
403 a significant up-regulation of essentially all cytokines and chemokines compared to  
404 controls. In general there was much higher cytokine production in microglia exposed to  
405 100ng-24h LPS conditioned media compared to 50ng-24hr LPS. We next determined if  
406 blockage of mitochondrial fission also modulated LPS-induced expression of cytokine and  
407 chemokine mediators. Mdivi-1 significantly reduced the pro-inflammatory cytokines (IL-  
408 1 $\alpha$ , IL-6, TNF- $\alpha$ , IL-12(p40)), chemokines (G-CSF, CCL5, RANTES) and anti-  
409 inflammatory cytokines (IL-10, IL-13) and the chemokines (monocyte chemotactic protein  
410 1 (MCP-1  $\beta$ ), in response to 100ng/ml of LPS for 24h. The LPS-induced production of IL-  
411 2, IL-5 and MIP1  $\alpha$  were not significantly reduced by Mdivi-1 (Fig.5).

412 **Mdivi-1 suppresses LPS induced succinate production.**

413 Succinate is a well-established pro-inflammatory metabolite that is known to accumulate  
414 during LPS induced macrophage activation (Mills et al., 2016) but the role of succinate  
415 during microglia activation needs further investigation. We found that LPS (100ng/ml)  
416 resulted in a significant increase of succinate (Fig.6a) accompanying the expression of  
417 pro/anti-inflammatory cytokines and chemokines. Mdivi-1 pretreatment (Fig 6a) or

418 blocking succinate production by succinate dehydrogenase inhibitor (DMM,10mM) (Fig.  
419 6b) normalized succinate production. These results were further strengthened by the fact  
420 that treatment with DMM or scavenging ROS production with NAC (10mM, 30 min)  
421 recapitulated the effects of Mdivi-1 (Fig.5) by reducing pro/anti-inflammatory cytokines  
422 and chemokine release (Supplementary figure S3). Excessive fission results in  
423 fragmented mitochondria and causes a metabolic shift in microglia (Khacho et al., 2014)  
424 from OCR to ECAR. This may result in increased succinate production which in turn acts  
425 as a feedback loop to amplify aberrant mitochondrial fission (Lu et al., 2018).

426 **Inhibition of mitochondria fission by Mdivi-1 suppresses mitochondrial ROS production.**

427 Mitochondrial ROS plays an important role in LPS-induced immune responses (Park et  
428 al., 2015). In order to examine the role of ROS production after LPS stimulation,  
429 mitochondrial ROS (mtROS) was measured with MitoSOX, a mitochondrial superoxide  
430 indicator. The fluorescence intensity of MitoSOX increased 24h after the LPS stimulation  
431 (100ng/ml, 24h) (Fig. 7). Treatment with Mdivi-1 (25  $\mu$ M, 1h) before LPS exposure  
432 abolished the increase in MitoSOX fluorescence intensity observed 2h after the LPS  
433 stimulation. These results indirectly show that that mitochondrial fission (induced by TLR4  
434 stimulation) increases ROS production as shown in this study and others (Kato et al.,  
435 2017; Park et al., 2013).

436 **Mdivi-1 treatment attenuated LPS induced increase of mitochondrial membrane**  
437 **potential**

438 Our data suggest that after LPS (100ng/ml) exposure for 24h microglia mainly depended  
439 on glycolysis for energy production. Therefore, we investigated the mitochondrial  
440 membrane potential using the mitochondrial membrane potential probe JC-1 in these  
441 conditions. We found that there was a consequent elevation of mitochondrial membrane  
442 potential and treatment with Mdivi-1 significantly reduced mitochondrial membrane  
443 potential (525/565 nm) ratio compared to LPS treated group (Fig. 8).

444 **Mdivi-1 treatment attenuated microglial activation in a mouse paradigm of**  
445 **neuroinflammation.**

446 Based on our working hypothesis that Mdivi-1 can reduce the inflammatory reaction of  
447 microglia, we sought to investigate the potential for Mdivi-1 to reduce the activation of  
448 microglia *in vivo* (Favrais et al., 2011; Krishnan et al., 2017). We isolated microglia from  
449 the brains of animals at P3 following induction of systemically driven neuroinflammation  
450 and con-current treatment with Mdivi-1 from P1-P3. We analyzed the isolated microglia  
451 for gene expression of markers associated with functional phenotypes including cytotoxic  
452 (*Nos2*, *Ptgs2*, *Cd32*), repair and regeneration (*Arg1*, *Lga3*, *Igf1*), and immunomodulatory  
453 (*Il1ra*, *Il4a*, *Socs3*) phenotypes. Exposure to neuroinflammatory-stimuli affected the gene  
454 expression as expected (Krishnan et al., 2017), with increased expression of all of the  
455 genes except for the gene for IGF1, which was decreased. IGF1 is a pleotropic growth

456 factor necessary for myelogenesis and known to be decreased by pro-inflammatory  
457 microglial activation (Wlodarczyk et al., 2017). Mdivi-1 treatment normalized to control  
458 (PBS) levels the expression of genes associated with cytotoxicity and  
459 immunomodulation, but had no effect on IGF1 gene expression, and only partly recovered  
460 Galectin-3 gene expression (*Lgal3*), indicating that exposure to Mdivi-1, which inhibits  
461 mitochondrial fragmentation, modulates the microglial inflammatory response also *in vivo*  
462 (Fig. 9).

### 463 **Discussion**

464 This study strengthens our knowledge of the links between mitochondrial architecture,  
465 inflammation and energy metabolism in microglial cells. We have shown that activation  
466 of microglia to a pro-inflammatory activation state increased mitochondrial fragmentation,  
467 which was accompanied by a reduction in oxidative phosphorylation and an increase in  
468 glycolysis, which was dose and time dependent. Pre-treatment with the putative  
469 mitochondrial division inhibitor, Mdivi-1, normalised LPS-induced mitochondrial  
470 fragmentation, normalised the cellular respiration and glycolysis to control levels. Mdivi-1  
471 greatly reduced LPS-induced cytokine production normalized LPS-induced ROS  
472 production and mitochondrial membrane potential.

473 Neuroinflammation includes complex changes in microglial phenotypes, mediated by  
474 gene expression changes leading to the production of cytokines and chemokines and  
475 production of ROS. Altogether this triggers oxidative and nitrosative stress in the brain

476 (Bolouri et al., 2014; Hellström Erkenstam et al., 2016). We observed as expected that  
477 LPS-activated microglia produced a plethora of chemokines and cytokines and ROS. In  
478 this pro-inflammatory scenario, suppression of LPS-induced mitochondrial ROS plays a  
479 role in modulating the production of pro-inflammatory mediators by preventing MAPK and  
480 NF- $\kappa$ B activation suggesting a potential therapy for inflammation-associated degenerative  
481 neurological diseases (Park et al., 2015).

482 To understand LPS-induced changes in mitochondrial structure, we used high resolution  
483 3D ELYRA-SIM (Shim et al., 2012) to quantify mitochondrial morphology which revealed  
484 that high dose LPS for 24h increased fragmentation. A low dose of LPS caused an initial  
485 increase in OCR which was not accompanied by any change in mitochondrial  
486 morphology. However, a higher dose of LPS induced a decrease of OCR and a further  
487 increase of ECAR which triggered mitochondrial fission. Fragmented mitochondria  
488 constitute the preferred morphological state when respiratory activity is low (Westermann,  
489 2012). A high or moderate dose of LPS caused a decrease in respiration and cells  
490 became dependent on glycolysis favoring excessive fragmentation. The molecular  
491 mechanisms behind this response is not known but it has been proposed that the energy  
492 depletion elicits mitochondrial fragmentation and subsequent mitophagy (Youle & van der  
493 Blik, 2012). Increased mitochondrial fragmentation due to excessive fission can  
494 exacerbate the inflammatory response of microglia (Ho et al., 2018) through modulation  
495 of DRP1 de-phosphorylation and elimination of ROS (Park et al., 2016). We chose to use

496 Mdivi-1 a mitochondrial division inhibitor to study microglial metabolism as it related to  
497 mitochondrial morphology as previous studies revealed that LPS exposure in microglia  
498 cells leads to activation of mitochondrial fission protein DRP1 (Kato et al., 2017; Park et  
499 al., 2013).

500 Mdivi-1 is a widely accepted DRP-1 mediated mitochondrial fission inhibitor used in many  
501 studies (Baek et al., 2017; Peiris-Pagès, Bonuccelli, Sotgia, & Lisanti, 2018; So, Hsing,  
502 Liang, & Wu, 2012; Xie et al., 2013) . Our data supports the assertion that changes in  
503 mitochondrial dynamics may be needed for the expression of inflammatory mediators in  
504 activated microglia cells. Mdivi-1 has previously been shown to attenuate LPS-induced  
505 ROS and proinflammatory mediator production in a BV-2 microglial cell line (Park et al.,  
506 2013) with a very high dose of 1ug/ml. BV2 cells are similar to primary microglia (Henn  
507 et al., 2009), but they contain oncogenes that render them phenotypically different with  
508 regard to e.g. proliferation and adhesion (Horvath, Nutile-McMenemy, Alkaitis, & Deleo,  
509 2008). Our findings not only show that pre-treatment with Mdivi-1 reduced LPS-induced  
510 mitochondrial fragmentation and expression of pro-inflammatory mediators, but also  
511 normalized mitochondrial function in microglia. These data support the suggestion that  
512 increasing the fusion/fission ratio reduces the extent of neuroinflammation (Kim, Lee,  
513 Park, Kim, & Roh, 2016). To further support the potential validity of targeting fission as a  
514 therapeutic strategy, we tested the ability of Mdivi-1 to modify microglial activity *in vivo*.  
515 We used a paradigm of systemically driven neuroinflammation, wherein an IP injection of

516 the inflammatory agent interleukin-1 $\beta$  induces a highly complex neuroinflammatory  
517 reaction involving microglia (Krishnan et al., 2017; Van Steenwinckel et al., 2018).  
518 Supporting our *in vitro* data mdivi-1 was able to reduce the expression of genes  
519 associated with classically pro-inflammatory genes, and the anti-inflammatory activation  
520 state, which is associated with the *in vivo* inflammatory reaction.

521 Previous work with BV2 demonstrated that LPS causes an inhibition of OXPHOS  
522 (Voloboueva, Emery, Sun, & Giffard, 2013). However, this study used a very high dose  
523 of LPS (1 $\mu$ g/ml) which is shown to elicit mitochondrial toxicity (Ahn et al., 2012). We  
524 demonstrate for the first time that a low or moderate dose of LPS (50ng/ml) results in an  
525 increase of ATP linked OCR and basal respiration in support of another study in skeletal  
526 muscle cells where they used a very low dose of LPS in isolated mitochondria (Frisard et  
527 al., 2015). High dose of LPS (100ng/ml) caused a decrease in FCCP induced maximal  
528 respiration and an increase in leak-driven respiration. A depletion of spare respiratory  
529 capacity was found at 6 and 24h following LPS exposure. However, we have noted no  
530 significant difference in cell viability or death after LPS.

531 OCR exhibited a biphasic response characterized initially by an increase of OCR in  
532 response to low LPS and then a marked drop of OCR after moderate to high doses of  
533 LPS whereas ECAR increased in proportion to the dose of LPS. We interpret the initial  
534 increase of OCR as a means to match an increased demand of ATP. However, as the  
535 pro-inflammatory stimulus becomes stronger it appears favourable to shift from

536 mitochondrial respiration to aerobic glycolysis (Warburg effect) in order to promote more  
537 rapid ATP production (Kelly & O'Neill, 2015; Orihuela et al., 2016) and synthesis of  
538 inflammatory mediators such as cytokines/chemokines and ROS (Kelly & O'Neill, 2015).  
539 We believe the Warburg effect is an important concept for understanding metabolic  
540 changes occurring during microglial activation. It is shown that also activation of  
541 macrophages or dendritic cells (DCs) with LPS, induces a metabolic switch from  
542 OXPHOS to glycolysis (Krawczyk et al., 2010). Metabolic shift may be facilitated by  
543 increased mitochondrial fission and/or reduced fusion mediated by DRP1 activation  
544 (Baker, Maitra, Geng, & Li, 2014). However, as glycolysis is less efficient at producing  
545 ATP than OXPHOS, this metabolic reorientation cannot solely be to meet energy  
546 demands. Glycolysis may also facilitate in cytokine production by producing intermediate  
547 metabolites (Mills et al., 2016). A previous study found that glycolysis was required to  
548 produce optimal IFN- $\gamma$  during T cell activation and is translationally regulated by the  
549 binding of the glycolysis enzyme GAPDH to IFN- $\gamma$  mRNA (Chang et al., 2013).

550 Our results in microglia add to what has already been shown in DCs and macrophages  
551 (Williams & O'Neill, 2018), specifically that pro-inflammatory activation resulted in  
552 increased succinate accumulation. In dendritic cells (DCs) and macrophages this  
553 succinate accumulation was related to an altered Krebs cycle and this was was  
554 normalized by Mdivi-1. Aberrant mitochondrial fission alters the Krebs cycle, by interfering  
555 with the processes after citrate and after succinate (Jha et al., 2015) by reducing of



556 cytochrome c oxidase and succinate dehydrogenase activity (B. Zhang et al., 2013).  
557 Impaired succinate dehydrogenase activity results in succinate accumulation due to  
558 impaired succinate to fumarate conversion (Mills et al., 2016). Accumulated succinate  
559 drives reverse electron transport (RET) to generate excessive mitochondrial ROS  
560 production (Chouchani et al., 2014; Niatsetskaya et al., 2012). Our data support this link  
561 between accumulation of succinate and ROS production, which was prevented by Mdivi-  
562 1.

563 LPS induced an increase in membrane potential and proton with an increase in  
564 membrane potential. Proton leak is partly mediated by uncoupling proteins (UCPs)  
565 present in the mitochondrial inner membrane (Hass & Barnstable, 2016; Krauss, Zhang,  
566 & Lowell, 2005). It is shown that in primary microglia LPS induces an increase in UCP2  
567 levels and membrane potential. UCP2-silenced microglia stimulated with LPS show a  
568 decrease in membrane potential (De Simone et al., 2015). In macrophages LPS  
569 stimulation repurpose their mitochondria from ATP production to succinate-dependent  
570 ROS generation, with glycolysis taking on the role of ATP generation. In this case  
571 mitochondria sustain a high membrane potential because protons generated by the  
572 electron transport chain to make ATP are no longer being consumed by mitochondrial  
573 ATP synthase (Mills et al., 2016). Macrophages can also reorganize their respiratory  
574 chain in response to a bacterial infection, decreasing Complex I levels and increasing  
575 the activity of Complex II (Garaude et al., 2016). These changes boost production of pro-

576 inflammatory cytokines such as interleukin 1 $\beta$  (IL-1 $\beta$ ) and IL-10. Our data support these  
577 findings as normalizing mitochondrial membrane potential and ROS production with  
578 Mdivi-1 abolished pro- and anti-inflammatory cytokine and chemokine release.

579 Aberrant activation of microglial affects neurodegenerative processes through various  
580 neurotoxic cascades. We have shown that pro-inflammatory microglial activation alters  
581 cellular bioenergetics by inducing mitochondrial dysfunction and promoting a switch to  
582 glycolysis, supported by excessive mitochondrial fragmentation and increased cytokine  
583 output. This is likely an adaptive mechanism as the transition of sensing and surveying  
584 microglia into an activated state is likely to be accompanied by significantly increased  
585 energy consumption. Preventing excessive mitochondrial fission in microglial cells  
586 stimulated with LPS using a fission inhibitor Mdivi-1 normalizes mitochondrial respiration  
587 and glycolysis and attenuates the release of cytokines/chemokines. These lines of *in*  
588 *vitro* morphological and functional data and the *in vivo* data suggest that regulating  
589 mitochondrial dynamics may be a useful therapeutic modality for preventing neurological  
590 disorders caused by aberrant microglia activation.

## 591 **References**

- 592 Ahn, S. K., Hong, S., Park, Y. M., Choi, J. Y., Lee, W. T., Park, K. A., & Lee, J. E.  
593 (2012). Protective effects of agmatine on lipopolysaccharide-injured microglia  
594 and inducible nitric oxide synthase activity. *Life Sciences*, *91*(25), 1345-1350.  
595 doi:<https://doi.org/10.1016/j.lfs.2012.10.010>
- 596 Baek, S. H., Park, S. J., Jeong, J. I., Kim, S. H., Han, J., Kyung, J. W., . . . Jo, D. G.  
597 (2017). Inhibition of Drp1 Ameliorates Synaptic Depression, Abeta Deposition,

- 598 and Cognitive Impairment in an Alzheimer's Disease Model. *J Neurosci*, *37*(20),  
599 5099-5110. doi:10.1523/jneurosci.2385-16.2017
- 600 Baker, B., Maitra, U., Geng, S., & Li, L. (2014). Molecular and Cellular Mechanisms  
601 Responsible for Cellular Stress and Low-grade Inflammation Induced by a Super-  
602 low Dose of Endotoxin. *J Biol Chem*, *289*(23), 16262-16269.  
603 doi:10.1074/jbc.M114.569210
- 604 Ball, G., Aljabar, P., Nongena, P., Kennea, N., Gonzalez-Cinca, N., Falconer, S., . . .  
605 Edwards, A. D. (2017). Multimodal image analysis of clinical influences on  
606 preterm brain development. *Annals of Neurology*. doi:10.1002/ana.24995
- 607 Bolouri, H., Savman, K., Wang, W., Thomas, A., Maurer, N., Dullaghan, E., . . . Mallard,  
608 C. (2014). Innate defense regulator peptide 1018 protects against perinatal brain  
609 injury. *Ann Neurol*, *75*(3), 395-410. doi:10.1002/ana.24087
- 610 Buck, M. D., O'Sullivan, D., Klein Geltink, R. I., Curtis, J. D., Chang, C. H., Sanin, D. E.,  
611 . . . Pearce, E. L. (2016). Mitochondrial Dynamics Controls T Cell Fate through  
612 Metabolic Programming. *Cell*, *166*(1), 63-76. doi:10.1016/j.cell.2016.05.035
- 613 Butovsky, O., & Weiner, H. L. (2018). Microglial signatures and their role in health and  
614 disease. *Nat Rev Neurosci*. doi:10.1038/s41583-018-0057-5
- 615 Cassidy-Stone, A., Chipuk, J. E., Ingerman, E., Song, C., Yoo, C., Kuwana, T., . . .  
616 Nunnari, J. (2008). Chemical inhibition of the mitochondrial division dynamin  
617 reveals its role in Bax/Bak-dependent mitochondrial outer membrane  
618 permeabilization. *Dev Cell*, *14*(2), 193-204. doi:10.1016/j.devcel.2007.11.019
- 619 Chang, C. H., Curtis, J. D., Maggi, L. B., Jr., Faubert, B., Villarino, A. V., O'Sullivan, D., .  
620 . . Pearce, E. L. (2013). Posttranscriptional control of T cell effector function by  
621 aerobic glycolysis. *Cell*, *153*(6), 1239-1251. doi:10.1016/j.cell.2013.05.016
- 622 Chhor, V., Le Charpentier, T., Lebon, S., Ore, M. V., Celador, I. L., Josserand, J., . . .  
623 Fleiss, B. (2013). Characterization of phenotype markers and neuronotoxic  
624 potential of polarised primary microglia in vitro. *Brain, Behavior, and Immunity*,  
625 *32*, 70-85. doi:10.1016/j.bbi.2013.02.005
- 626 Chouchani, E. T., Pell, V. R., Gaude, E., Aksentijević, D., Sundier, S. Y., Robb, E. L., . .  
627 . Murphy, M. P. (2014). Ischaemic accumulation of succinate controls reperfusion

- 628 injury through mitochondrial ROS. *Nature*, *515*(7527), 431-435.  
629 doi:10.1038/nature13909
- 630 De Simone, R., Ajmone-Cat, M. A., Pandolfi, M., Bernardo, A., De Nuccio, C., Minghetti,  
631 L., & Visentin, S. (2015). The mitochondrial uncoupling protein-2 is a master  
632 regulator of both M1 and M2 microglial responses. *J Neurochem*, *135*(1), 147-  
633 156. doi:10.1111/jnc.13244
- 634 Dean, J. M., Wang, X., Kaindl, A. M., Gressens, P., Fleiss, B., Hagberg, H., & Mallard,  
635 C. (2010). Microglial MyD88 signaling regulates acute neuronal toxicity of LPS-  
636 stimulated microglia in vitro. *Brain Behav Immun*, *24*(5), 776-783.  
637 doi:10.1016/j.bbi.2009.10.018
- 638 Everts, B., Amiel, E., Huang, S. C.-C., Smith, A. M., Chang, C.-H., Lam, W. Y., . . .  
639 Pearce, E. J. (2014). TLR-driven early glycolytic reprogramming via the kinases  
640 TBK1-IKK $\epsilon$  supports the anabolic demands of dendritic cell activation. *Nat*  
641 *Immunol*, *15*(4), 323-332. doi:10.1038/ni.2833
- 642 Favrais, G., van de Looij, Y., Fleiss, B., Ramanantsoa, N., Bonnin, P., Stoltenburg-  
643 Didinger, G., . . . Gressens, P. (2011). Systemic inflammation disrupts the  
644 developmental program of white matter. *Annals of Neurology*, *70*(4), 550-565.  
645 doi:10.1002/ana.22489
- 646 Frezza, C., Cipolat, S., Martins de Brito, O., Micaroni, M., Beznoussenko, G. V., Rudka,  
647 T., . . . Scorrano, L. (2006). OPA1 controls apoptotic cristae remodeling  
648 independently from mitochondrial fusion. *Cell*, *126*(1), 177-189.  
649 doi:10.1016/j.cell.2006.06.025
- 650 Frisard, M. I., Wu, Y., McMillan, R. P., Voelker, K. A., Wahlberg, K. A., Anderson, A. S.,  
651 . . . Hulver, M. W. (2015). Low levels of lipopolysaccharide modulate  
652 mitochondrial oxygen consumption in skeletal muscle. *Metabolism: clinical and*  
653 *experimental*, *64*(3), 416-427. doi:10.1016/j.metabol.2014.11.007
- 654 Garaude, J., Acin-Perez, R., Martinez-Cano, S., Enamorado, M., Ugolini, M., Nistal-  
655 Villan, E., . . . Sancho, D. (2016). Mitochondrial respiratory-chain adaptations in  
656 macrophages contribute to antibacterial host defense. *Nat Immunol*, *17*(9), 1037-  
657 1045. doi:10.1038/ni.3509

- 658 Gimeno-Bayon, J., Lopez-Lopez, A., Rodriguez, M. J., & Mahy, N. (2014). Glucose  
659 pathways adaptation supports acquisition of activated microglia phenotype. *J*  
660 *Neurosci Res*, *92*(6), 723-731. doi:10.1002/jnr.23356
- 661 Greter, M., Lelios, I., & Croxford, A. L. (2015). Microglia Versus Myeloid Cell  
662 Nomenclature during Brain Inflammation. *Frontiers in Immunology*, *6*, 249.  
663 doi:10.3389/fimmu.2015.00249
- 664 Hackenbrock, C. R. (1966). Ultrastructural bases for metabolically linked mechanical  
665 activity in mitochondria. I. Reversible ultrastructural changes with change in  
666 metabolic steady state in isolated liver mitochondria. *J Cell Biol*, *30*(2), 269-297.
- 667 Hagberg, H., Mallard, C., Rousset, C. I., & Thornton, C. (2014). Mitochondria: hub of  
668 injury responses in the developing brain. *Lancet Neurol*, *13*(2), 217-232.  
669 doi:10.1016/s1474-4422(13)70261-8
- 670 Hass, D. T., & Barnstable, C. J. (2016). Uncoupling protein 2 in the glial response to  
671 stress: implications for neuroprotection. *Neural regeneration research*, *11*(8),  
672 1197-1200. doi:10.4103/1673-5374.189159
- 673 Hellström Erkenstam, N., Smith, P. L. P., Fleiss, B., Nair, S., Svedin, P., Wang, W., . . .  
674 Mallard, C. (2016). Temporal Characterization of Microglia/Macrophage  
675 Phenotypes in a Mouse Model of Neonatal Hypoxic-Ischemic Brain Injury.  
676 *Frontiers in Cellular Neuroscience*, *10*, 286. doi:10.3389/fncel.2016.00286
- 677 Henn, A., Lund, S., Hedtjarn, M., Schratzenholz, A., Porzgen, P., & Leist, M. (2009). The  
678 suitability of BV2 cells as alternative model system for primary microglia cultures  
679 or for animal experiments examining brain inflammation. *ALTEX*, *26*(2), 83-94.
- 680 Ho, D. H., Je, A. R., Lee, H., Son, I., Kweon, H. S., Kim, H. G., & Seol, W. (2018).  
681 LRRK2 Kinase Activity Induces Mitochondrial Fission in Microglia via Drp1 and  
682 Modulates Neuroinflammation. *Exp Neurobiol*, *27*(3), 171-180.  
683 doi:10.5607/en.2018.27.3.171
- 684 Horvath, R. J., Nutile-McMenemy, N., Alkaitis, M. S., & Deleo, J. A. (2008). Differential  
685 migration, LPS-induced cytokine, chemokine, and NO expression in immortalized  
686 BV-2 and HAPI cell lines and primary microglial cultures. *J Neurochem*, *107*(2),  
687 557-569. doi:10.1111/j.1471-4159.2008.05633.x

- 688 Huang, B., Bates, M., & Zhuang, X. (2009). Super resolution fluorescence microscopy.  
689 *Annual review of biochemistry*, *78*, 993-1016.  
690 doi:10.1146/annurev.biochem.77.061906.092014
- 691 Jahani-Asl, A., Pilon-Larose, K., Xu, W., MacLaurin, J. G., Park, D. S., McBride, H. M.,  
692 & Slack, R. S. (2011). The mitochondrial inner membrane GTPase, optic atrophy  
693 1 (Opa1), restores mitochondrial morphology and promotes neuronal survival  
694 following excitotoxicity. *J Biol Chem*, *286*(6), 4772-4782.  
695 doi:10.1074/jbc.M110.167155
- 696 Jha, Abhishek K., Huang, Stanley C.-C., Sergushichev, A., Lampropoulou, V., Ivanova,  
697 Y., Loginicheva, E., . . . Artyomov, Maxim N. (2015). Network Integration of  
698 Parallel Metabolic and Transcriptional Data Reveals Metabolic Modules that  
699 Regulate Macrophage Polarization. *Immunity*, *42*(3), 419-430.  
700 doi:<https://doi.org/10.1016/j.immuni.2015.02.005>
- 701 Katoh, M., Wu, B., Nguyen, H. B., Thai, T. Q., Yamasaki, R., Lu, H., . . . Ohno, N.  
702 (2017). Polymorphic regulation of mitochondrial fission and fusion modifies  
703 phenotypes of microglia in neuroinflammation. *Scientific Reports*, *7*(1), 4942.  
704 doi:10.1038/s41598-017-05232-0
- 705 Kelly, B., & O'Neill, L. A. J. (2015). Metabolic reprogramming in macrophages and  
706 dendritic cells in innate immunity. *Cell Research*, *25*(7), 771-784.  
707 doi:10.1038/cr.2015.68
- 708 Khacho, M., Tarabay, M., Patten, D., Khacho, P., MacLaurin, J. G., Guadagno, J., . . .  
709 Slack, R. S. (2014). Acidosis overrides oxygen deprivation to maintain  
710 mitochondrial function and cell survival. *Nat Commun*, *5*, 3550.  
711 doi:10.1038/ncomms4550
- 712 Kim, H., Lee, J. Y., Park, K. J., Kim, W.-H., & Roh, G. S. (2016). A mitochondrial  
713 division inhibitor, Mdivi-1, inhibits mitochondrial fragmentation and attenuates  
714 kainic acid-induced hippocampal cell death. *BMC Neuroscience*, *17*, 33.  
715 doi:10.1186/s12868-016-0270-y
- 716 Koning, G., Leverin, A. L., Nair, S., Schwendimann, L., Ek, J., Carlsson, Y., . . .  
717 Hagberg, H. (2017). Magnesium induces preconditioning of the neonatal brain

- 718 via profound mitochondrial protection. *J Cereb Blood Flow Metab*,  
719 271678x17746132. doi:10.1177/0271678x17746132
- 720 Krauss, S., Zhang, C.-Y., & Lowell, B. B. (2005). The mitochondrial uncoupling-protein  
721 homologues. *Nature Reviews Molecular Cell Biology*, 6, 248.  
722 doi:10.1038/nrm1592
- 723 Krawczyk, C. M., Holowka, T., Sun, J., Blagih, J., Amiel, E., DeBerardinis, R. J., . . .  
724 Pearce, E. J. (2010). Toll-like receptor-induced changes in glycolytic metabolism  
725 regulate dendritic cell activation. *Blood*, 115(23), 4742-4749. doi:10.1182/blood-  
726 2009-10-249540
- 727 Krishnan, M. L., Van Steenwinckel, J., Schang, A. L., Yan, J., Arnadottir, J., Le  
728 Charpentier, T., . . . Gressens, P. (2017). Integrative genomics of microglia  
729 implicates DLG4 (PSD95) in the white matter development of preterm infants.  
730 *Nat Commun*, 8(1), 428. doi:10.1038/s41467-017-00422-w
- 731 Leaw, B., Nair, S., Lim, R., Thornton, C., Mallard, C., & Hagberg, H. (2017).  
732 Mitochondria, Bioenergetics and Excitotoxicity: New Therapeutic Targets in  
733 Perinatal Brain Injury. *Frontiers in Cellular Neuroscience*, 11(199).  
734 doi:10.3389/fncel.2017.00199
- 735 Lu, Y.-T., Li, L.-Z., Yang, Y.-L., Yin, X., Liu, Q., Zhang, L., . . . Qi, L.-W. (2018).  
736 Succinate induces aberrant mitochondrial fission in cardiomyocytes through  
737 GPR91 signaling. *Cell Death & Disease*, 9(6), 672. doi:10.1038/s41419-018-  
738 0708-5
- 739 Mills, E. L., Kelly, B., Logan, A., Costa, A. S., Varma, M., Bryant, C. E., . . . O'Neill, L. A.  
740 (2016). Succinate Dehydrogenase Supports Metabolic Repurposing of  
741 Mitochondria to Drive Inflammatory Macrophages. *Cell*, 167(2), 457-470 e413.  
742 doi:10.1016/j.cell.2016.08.064
- 743 Moss, D. W., & Bates, T. E. (2001). Activation of murine microglial cell lines by  
744 lipopolysaccharide and interferon-gamma causes NO-mediated decreases in  
745 mitochondrial and cellular function. *Eur J Neurosci*, 13(3), 529-538.
- 746 Mottahedin, A., Svedin, P., Nair, S., Mohn, C. J., Wang, X., Hagberg, H., . . . Mallard, C.  
747 (2017). Systemic activation of Toll-like receptor 2 suppresses mitochondrial

- 748 respiration and exacerbates hypoxic-ischemic injury in the developing brain. *J*  
749 *Cereb Blood Flow Metab*, 271678x17691292. doi:10.1177/0271678x17691292
- 750 Nasrallah, C. M., & Horvath, T. L. (2014). Mitochondrial dynamics in the central  
751 regulation of metabolism. *Nat Rev Endocrinol*, 10(11), 650-658.  
752 doi:10.1038/nrendo.2014.160
- 753 Niatetskaya, Z. V., Sosunov, S. A., Matsiukevich, D., Utkina-Sosunova, I. V., Ratner,  
754 V. I., Starkov, A. A., & Ten, V. S. (2012). The oxygen free radicals originating  
755 from mitochondrial complex I contribute to oxidative brain injury following  
756 hypoxia-ischemia in neonatal mice. *J Neurosci*, 32(9), 3235-3244.  
757 doi:10.1523/jneurosci.6303-11.2012
- 758 Orihuela, R., McPherson, C. A., & Harry, G. J. (2016). Microglial M1/M2 polarization and  
759 metabolic states. *Br J Pharmacol*, 173(4), 649-665. doi:10.1111/bph.13139
- 760 Park, J., Choi, H., Kim, B., Chae, U., Lee, D. G., Lee, S. R., . . . Lee, D. S. (2016).  
761 Peroxiredoxin 5 (Prx5) decreases LPS-induced microglial activation through  
762 regulation of Ca(2+)/calcineurin-Drp1-dependent mitochondrial fission. *Free*  
763 *Radic Biol Med*, 99, 392-404. doi:10.1016/j.freeradbiomed.2016.08.030
- 764 Park, J., Choi, H., Min, J. S., Park, S. J., Kim, J. H., Park, H. J., . . . Lee, D. S. (2013).  
765 Mitochondrial dynamics modulate the expression of pro-inflammatory mediators  
766 in microglial cells. *J Neurochem*, 127(2), 221-232. doi:10.1111/jnc.12361
- 767 Park, J., Min, J. S., Kim, B., Chae, U. B., Yun, J. W., Choi, M. S., . . . Lee, D. S. (2015).  
768 Mitochondrial ROS govern the LPS-induced pro-inflammatory response in  
769 microglia cells by regulating MAPK and NF-kappaB pathways. *Neurosci Lett*,  
770 584, 191-196. doi:10.1016/j.neulet.2014.10.016
- 771 Peacock, J. L., Marston, L., Marlow, N., Calvert, S. A., & Greenough, A. (2012).  
772 Neonatal and infant outcome in boys and girls born very prematurely. *Pediatric*  
773 *Research*, 71(3), 305-310. doi:10.1038/pr.2011.50
- 774 Peiris-Pagès, M., Bonuccelli, G., Sotgia, F., & Lisanti, M. P. (2018). Mitochondrial fission  
775 as a driver of stemness in tumor cells: mDIVI1 inhibits mitochondrial function, cell  
776 migration and cancer stem cell (CSC) signalling. *Oncotarget*, 9(17), 13254-  
777 13275. doi:10.18632/oncotarget.24285



- 778 Pickles, S., Vigie, P., & Youle, R. J. (2018). Mitophagy and Quality Control Mechanisms  
779 in Mitochondrial Maintenance. *Curr Biol*, *28*(4), R170-r185.  
780 doi:10.1016/j.cub.2018.01.004
- 781 Raju, T. N. K., Buist, A. S., Blaisdell, C. J., Moxey-Mims, M., & Saigal, S. (2017). Adults  
782 born preterm: a review of general health and system-specific outcomes. *Acta*  
783 *Paediatrica*. doi:10.1111/apa.13880
- 784 Ruiz, A., Alberdi, E., & Matute, C. (2018). Mitochondrial Division Inhibitor 1 (mdivi-1)  
785 Protects Neurons against Excitotoxicity through the Modulation of Mitochondrial  
786 Function and Intracellular Ca(2+) Signaling. *Frontiers in Molecular Neuroscience*,  
787 *11*, 3. doi:10.3389/fnmol.2018.00003
- 788 Schang, A.-L., Van Steenwinckel, J., Chevenne, D., Alkmark, M., Hagberg, H.,  
789 Gressens, P., & Fleiss, B. (2014). Failure of thyroid hormone treatment to  
790 prevent inflammation-induced white matter injury in the immature brain. *Brain*  
791 *Behav Immun*, *37*(100), 95-102. doi:10.1016/j.bbi.2013.11.005
- 792 Schuster, S., Boley, D., Moller, P., Stark, H., & Kaleta, C. (2015). Mathematical models  
793 for explaining the Warburg effect: a review focussed on ATP and biomass  
794 production. *Biochem Soc Trans*, *43*(6), 1187-1194. doi:10.1042/bst20150153
- 795 Shim, S. H., Xia, C., Zhong, G., Babcock, H. P., Vaughan, J. C., Huang, B., . . . Zhuang,  
796 X. (2012). Super-resolution fluorescence imaging of organelles in live cells with  
797 photoswitchable membrane probes. *Proc Natl Acad Sci U S A*, *109*(35), 13978-  
798 13983. doi:10.1073/pnas.1201882109
- 799 Shiow, L. R., Favrais, G., Schirmer, L., Schang, A. L., Cipriani, S., Andres, C., . . .  
800 Rowitch, D. H. (2017). Reactive astrocyte COX2-PGE2 production inhibits  
801 oligodendrocyte maturation in neonatal white matter injury. *Glia*, *65*(12), 2024-  
802 2037. doi:10.1002/glia.23212
- 803 Shitara, H., Kaneda, H., Sato, A., Iwasaki, K., Hayashi, J., Taya, C., & Yonekawa, H.  
804 (2001). Non-invasive visualization of sperm mitochondria behavior in transgenic  
805 mice with introduced green fluorescent protein (GFP). *FEBS Lett*, *500*(1-2), 7-11.
- 806 So, E. C., Hsing, C. H., Liang, C. H., & Wu, S. N. (2012). The actions of mdivi-1, an  
807 inhibitor of mitochondrial fission, on rapidly activating delayed-rectifier K(+)

- 808 current and membrane potential in HL-1 murine atrial cardiomyocytes. *Eur J*  
809 *Pharmacol*, 683(1-3), 1-9. doi:10.1016/j.ejphar.2012.02.012
- 810 Solito, E., & Sastre, M. (2012). Microglia Function in Alzheimer's Disease. *Frontiers in*  
811 *Pharmacology*, 3, 14. doi:10.3389/fphar.2012.00014
- 812 Song, Z., Ghochani, M., McCaffery, J. M., Frey, T. G., & Chan, D. C. (2009). Mitofusins  
813 and OPA1 mediate sequential steps in mitochondrial membrane fusion. *Mol Biol*  
814 *Cell*, 20(15), 3525-3532. doi:10.1091/mbc.E09-03-0252
- 815 Tay, T. L., Savage, J. C., Hui, C. W., Bisht, K., & Tremblay, M. E. (2017). Microglia  
816 across the lifespan: from origin to function in brain development, plasticity and  
817 cognition. *J Physiol*, 595(6), 1929-1945. doi:10.1113/JP272134
- 818 Thion, M. S., Low, D., Silvin, A., Chen, J., Grisel, P., Schulte-Schrepping, J., . . . Garel,  
819 S. (2018). Microbiome Influences Prenatal and Adult Microglia in a Sex-Specific  
820 Manner. *Cell*, 172(3), 500-516.e516. doi:10.1016/j.cell.2017.11.042
- 821 Wai, T., & Langer, T. (2016). Mitochondrial Dynamics and Metabolic Regulation. *Trends*  
822 *in Endocrinology & Metabolism*, 27(2), 105-117.  
823 doi:<https://doi.org/10.1016/j.tem.2015.12.001>
- 824 Van Steenwinckel, J., Schang, A. L., Krishnan, M. L., Degos, V., Delahaye-Duriez, A.,  
825 Bokobza, C., . . . Gressens, P. (2018). Loss of the Wnt/ $\beta$ -catenin pathway in  
826 microglia of the developing brain drives pro-inflammatory activation leading to  
827 white matter injury. *Biorxiv preprint*. doi:<https://doi.org/10.1101/334359>
- 828 Westermann, B. (2012). Bioenergetic role of mitochondrial fusion and fission. *Biochim*  
829 *Biophys Acta*, 1817(10), 1833-1838. doi:10.1016/j.bbabi.2012.02.033
- 830 Williams, N. C., & O'Neill, L. A. J. (2018). A Role for the Krebs Cycle Intermediate  
831 Citrate in Metabolic Reprogramming in Innate Immunity and Inflammation.  
832 *Frontiers in Immunology*, 9(141). doi:10.3389/fimmu.2018.00141
- 833 Wlodarczyk, A., Holtman, I. R., Krueger, M., Yogev, N., Bruttger, J., Khorrooshi, R., . . .  
834 Owens, T. (2017). A novel microglial subset plays a key role in myelinogenesis in  
835 developing brain. *EMBO Journal*. doi:10.15252/embj.201696056
- 836 Voloboueva, L. A., Emery, J. F., Sun, X., & Giffard, R. G. (2013). Inflammatory response  
837 of microglial BV-2 cells includes a glycolytic shift and is modulated by

- 838 mitochondrial glucose-regulated protein 75/mortalin. *FEBS Lett*, *587*(6), 756-762.  
839 doi:10.1016/j.febslet.2013.01.067
- 840 Wu, M., Neilson, A., Swift, A. L., Moran, R., Tamagnine, J., Parslow, D., . . . Ferrick, D.  
841 A. (2007). Multiparameter metabolic analysis reveals a close link between  
842 attenuated mitochondrial bioenergetic function and enhanced glycolysis  
843 dependency in human tumor cells. *Am J Physiol Cell Physiol*, *292*(1), C125-136.  
844 doi:10.1152/ajpcell.00247.2006
- 845 Xie, N., Wang, C., Lian, Y., Zhang, H., Wu, C., & Zhang, Q. (2013). A selective inhibitor  
846 of Drp1, mdivi-1, protects against cell death of hippocampal neurons in  
847 pilocarpine-induced seizures in rats. *Neurosci Lett*, *545*, 64-68.  
848 doi:10.1016/j.neulet.2013.04.026
- 849 Youle, R. J., & van der Bliek, A. M. (2012). Mitochondrial fission, fusion, and stress.  
850 *Science (New York, N.Y.)*, *337*(6098), 1062-1065. doi:10.1126/science.1219855
- 851 Zhang, B., Davidson, M. M., Zhou, H., Wang, C., Walker, W. F., & Hei, T. K. (2013).  
852 Cytoplasmic irradiation results in mitochondrial dysfunction and DRP1-dependent  
853 mitochondrial fission. *Cancer Res*, *73*(22), 6700-6710. doi:10.1158/0008-  
854 5472.can-13-1411
- 855 Zhang, Y., Liao, S., Yang, M., Liang, X., Poon, M. W., Wong, C. Y., . . . Lian, Q. (2012).  
856 Improved cell survival and paracrine capacity of human embryonic stem cell-  
857 derived mesenchymal stem cells promote therapeutic potential for pulmonary  
858 arterial hypertension. *Cell Transplant*, *21*(10), 2225-2239.  
859 doi:10.3727/096368912x653020
- 860

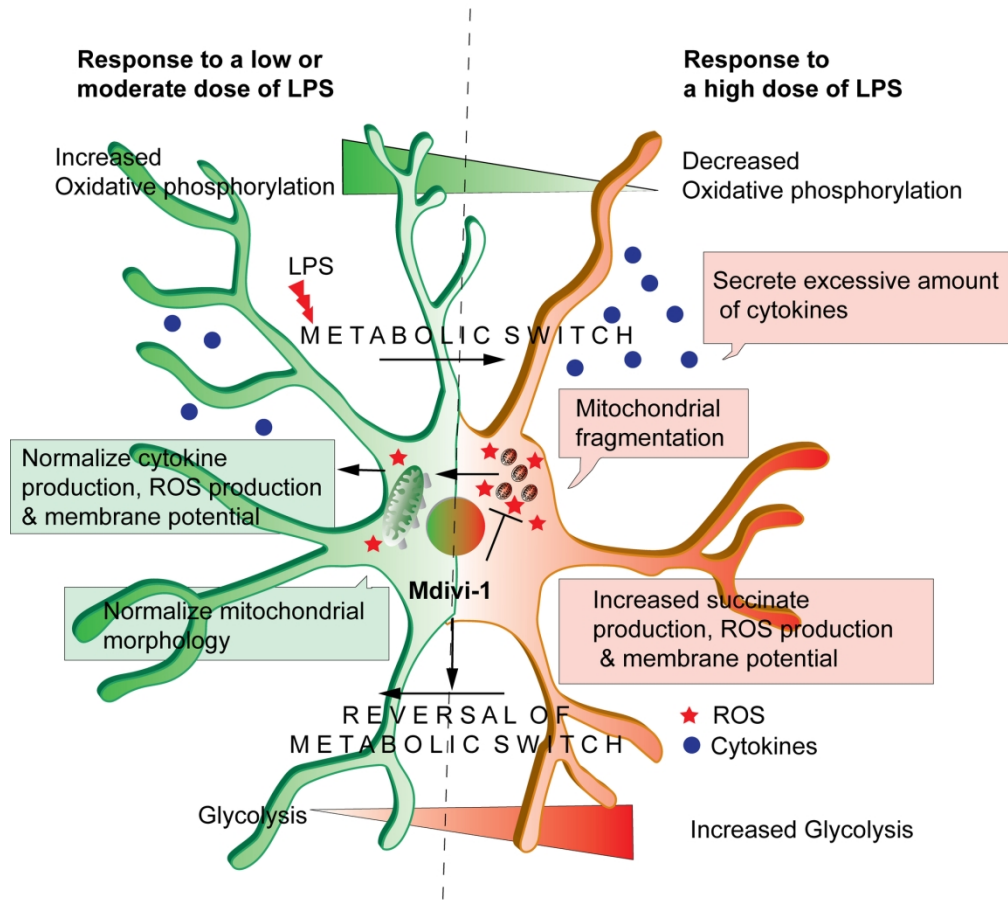


Table of Contents Image (TOCI)

173x169mm (300 x 300 DPI)

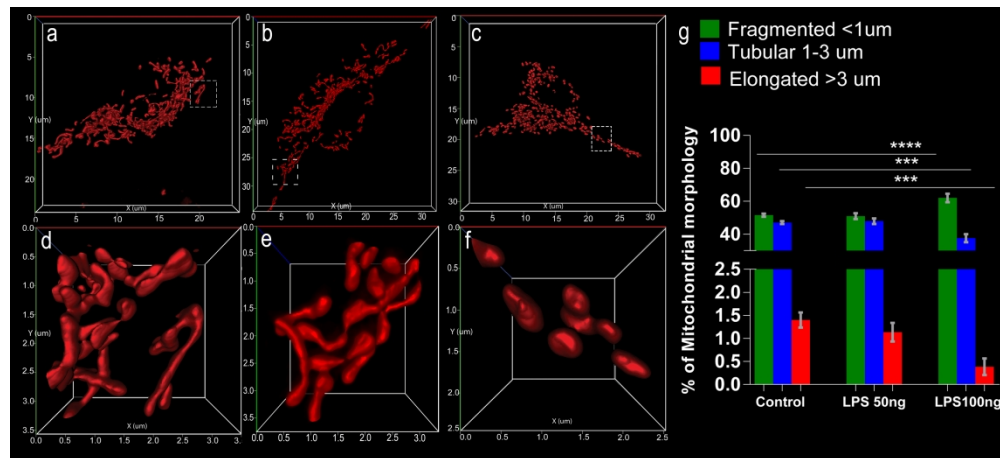


Fig:1 LPS induces dose-dependent mitochondrial fragmentation. Super-resolution microscopy reveals excessive mitochondrial fragmentation (a) Control (b) 50ng/ml LPS exposure for 24hrs (c) 100ng/ml LPS exposure for 24hrs (d-f) shows a higher magnification of the image in the white square in the upper panel. (g) Graphs showing results from an analysis of mitochondria morphology in primary microglia cells treated with LPS for 24h. The data are for at least 12 cells per condition in three independent experiments. Bar graphs expressed as mean  $\pm$  SEM. \*\*\*\* $P \leq 0.001$ ; student-t test calculating the difference between control and LPS treated groups.

344x157mm (300 x 300 DPI)

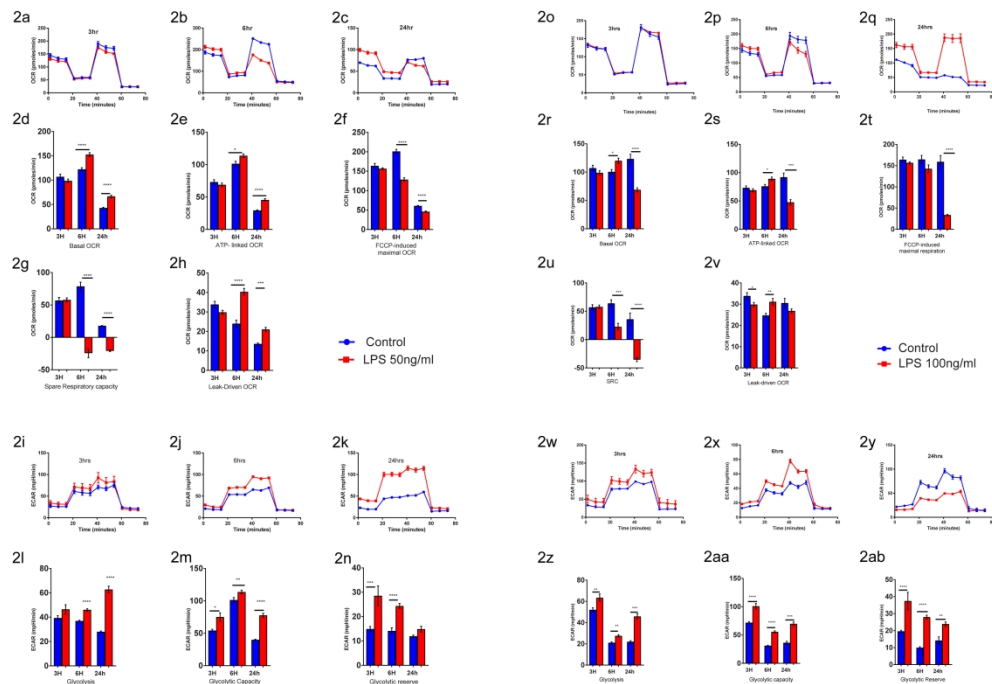


Fig:2 LPS dependent metabolic shift. Low dose of LPS (50 ng/ml) induces an increase in mitochondrial respiration and glycolysis: 50ng/ml LPS treatment shows an increase in Basal OCR, ATP linked OCR (d-e) whereas FCCP linked maximal OCR (f) and spare respiratory capacity (g) decreased from 3- 24hrs. Leak-driven OCR was also increased from 6-24hrs. Glycolytic parameters, based on ECAR, tended to increase from 3-24hrs (i-n). Whereas a high dose (100ng/ml) of LPS induces a time dependent metabolic shift. 100ng/ml LPS treatment for 6h shows an increase in Basal OCR, ATP linked OCR, while LPS treatment for 24h resulted in a decrease of Basal and ATP linked OCR (r-s). FCCP linked maximal OCR (t) and spare respiratory capacity (u) decreased from 6- 24hrs. Leak driven OCR was increased at 6 hrs (v). OCR and ECAR measured for 3,6 and 24hrs are expressed in bar graph format as the mean  $\pm$  SEM n=9. \*P  $\leq$  0.05; \*\*P  $\leq$  0.01; \*\*\*P  $\leq$  0.001 student t test calculating the difference between control and LPS treated groups.

298x202mm (300 x 300 DPI)

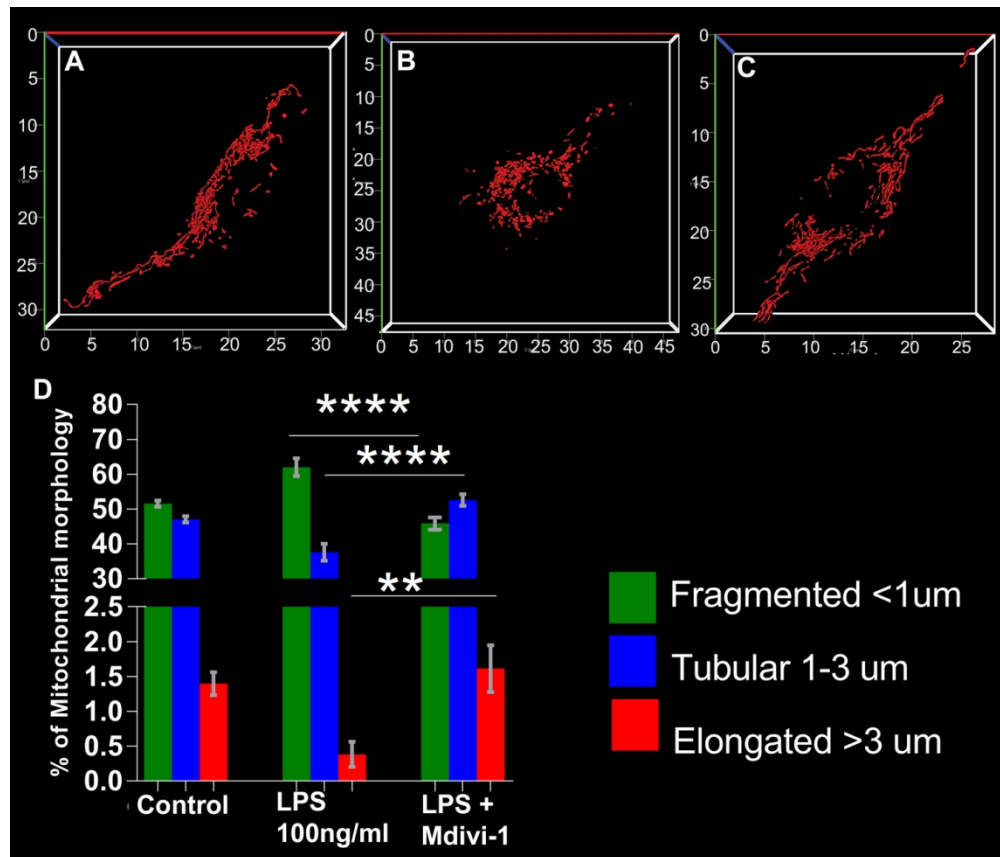


Fig.3 Pharmacologic blockade of DRP1 by Mdivi-1 re-established mitochondrial morphology. Mdivi-1 pre-treatment (25µm) for 1hr followed by LPS (100ng/ml) exposure for 24h resulted in a decrease of fragmented mitochondria and an increase in tubular and elongated mitochondria (d). A-Control cells treated with vehicle (DMSO), B- LPS (100ng/ml) exposure for 24h, C- LPS (100ng/ml)+ Mdivi-1. Bar graphs expressed as mean  $\pm$  SEM. The data are for at least 12 cells per condition in three independent experiments. \*\*P  $\leq$  0.01; \*\*\*\*P  $\leq$  0.001; student-t test calculating the difference between LPS and LPS+Mdivi-1 groups.

126x108mm (300 x 300 DPI)

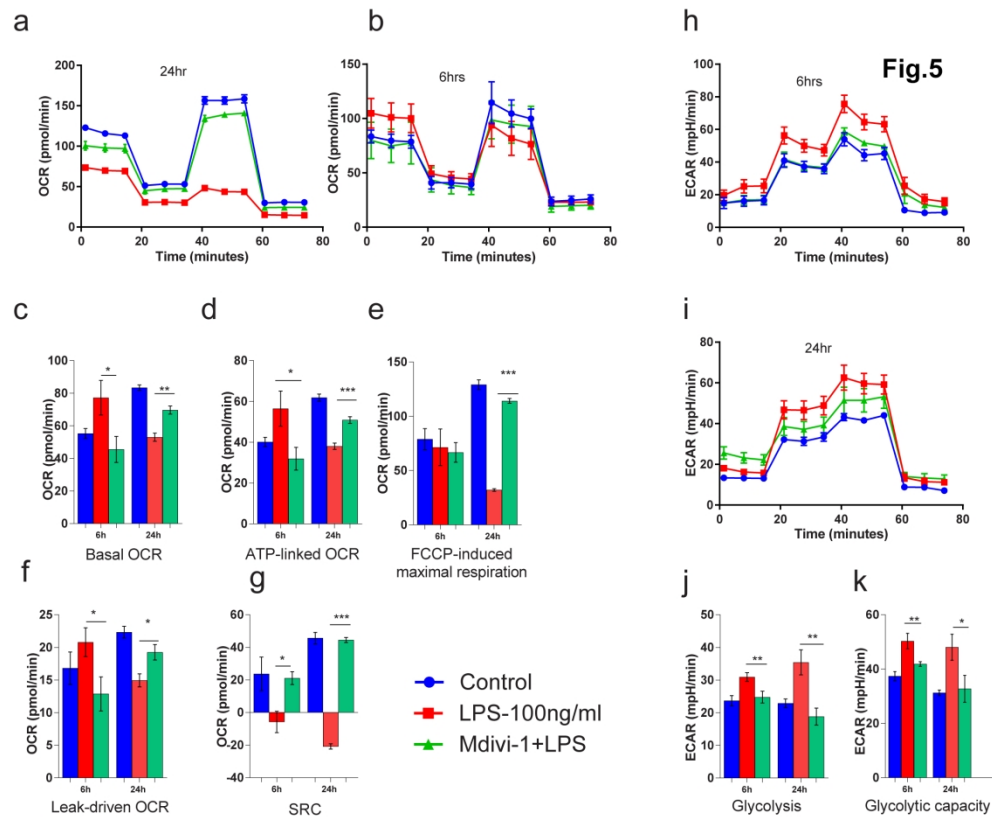


Fig.4 Mdivi-1 treatment reversed the metabolic shift. Inhibition of DRP1 by Mdivi-1 resulted in reduced basal OCR and ATP-linked OCR at 6h whereas Mdivi-1 increased basal OCR and ATP-linked OCR at 24h compared to 100ng/ml LPS exposure (c-d). LPS induced reduction in FCCP-induced maximal respiration and Leak-driven OCR at 24hr, which was normalized by Mdivi-1 (e-f). The LPS-evoked drop in SRC was prevented by Mdivi-1 (g). Mdivi-1 normalized LPS-induced increased ECAR dependent glycolysis and glycolytic capacity (j-h). OCR and ECAR measured for 3, 6 and 24hrs are expressed in bar graph format as the mean  $\pm$  SEM n=6-9. \*\*\*P  $\leq$  0.001; student-t test calculating the difference between LPS and LPS+Mdivi-1 treated groups.



	Control	Contol+Mdivi-1	LPS-100ng/ml	LPS+Mdivi-1	
17.26	18.39	518.30	411.01*	IL-1a	
833.62	788.36	3197.05	2751.92***	IL-1b	
0.72	1.68	12.21	12.13	IL-2	
3.16	3.51	60.20	43.31***	IL-3	
23.83	23.94	90.86	79.13***	IL-4	
0.34	0.34	25.86	21.10	IL-5	
3.66	4.98	8099.09	5505.45*	IL-6	
406.21	281.27	1430	1213.83***	IL-9	
46.01	40.44	418.38	326.98***	IL-10	
8.70	9.09	14195.76	9055.49***	IL-12 (p40)	
214.17	237.21	2252.40	1834.83**	IL-12 (p70)	
244.74	221.31	1495.88	1202.81***	IL-13	
3.09	2.40	27.05	21.27**	IL-17	
270.70	1598.25	29294.70	24062.81**	Eotaxin	
13.36	21.26	128234.46	24062.25*	G-CSF	
33.19	36.51	393.39	360.24*	GM-CSF	
13.24	15.56	97.27	77.43**	IFN-g	
23.08	19.04	24446.02	17194.63*	KC	
1567.31	1447.61	41681.24	9950.50***	MCP-1	
2725.74	2350.30	3020223.30	315229.38	MIP-1a	
8290.00	6994.69	163583.01	79899.81***	MIP-1b	
17.07	15.56	11108.15	6345.64***	RANTES	
49.36	45.73	117556.04	68721.20***	TNF-a	

Fig.5 Mdivi-1 treatment abolished LPS induced exaggerated pro/anti cytokine and chemokine response. Microglia cells were pre-treated with Mdivi-1 (25 $\mu$ M) for one hour followed by LPS (100ng/ml) for 24h, MCM were collected and analysed by 23-plex cytokine assay. Heat maps show cytokine concentration (pg/ml). KC = keratinocyte chemoattractant. n=8 \*P  $\leq$  0.05; \*\*P  $\leq$  0.01; \*\*\*P  $\leq$  0.001; student-t test calculating the difference between LPS and LPS+Mdivi-1 treated groups.

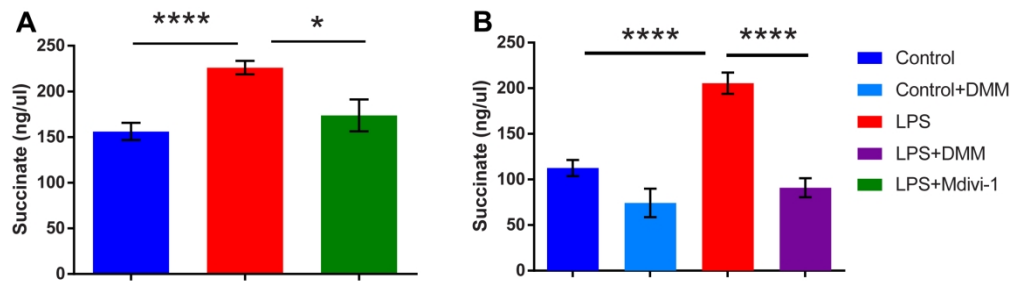


Fig.6 (A) Mdivi-1 normalized LPS induced succinate upregulation. Microglia cell homogenates of cells were analysed by succinate colorimetric assay. Microglia cells were pre-treated with Mdivi-1 (25uM; 1h) followed by LPS exposure of 100ng LPS for 24h resulted in significant downregulation of LPS induced succinate upregulation. Bar graph expressed as the mean  $\pm$  SEM n=8. \* $P \leq 0.05$ ; student-t test calculating the difference between LPS and LPS+Mdivi-1 treated groups. (B) Succinate dehydrogenase inhibitor recapitulated the effects of Mdivi-1. Pre-treatment with dimethyl malonate (DMM, 10mM; 3h) prior to LPS exposure attenuated succinate accumulation. Bar graph format as the mean  $\pm$  SEM n=9. \* $P \leq 0.05$ , Turkey's post-hoc test using One-Way Anova revealed difference between control, control + DMM, LPS and LPS+DMM treated groups.

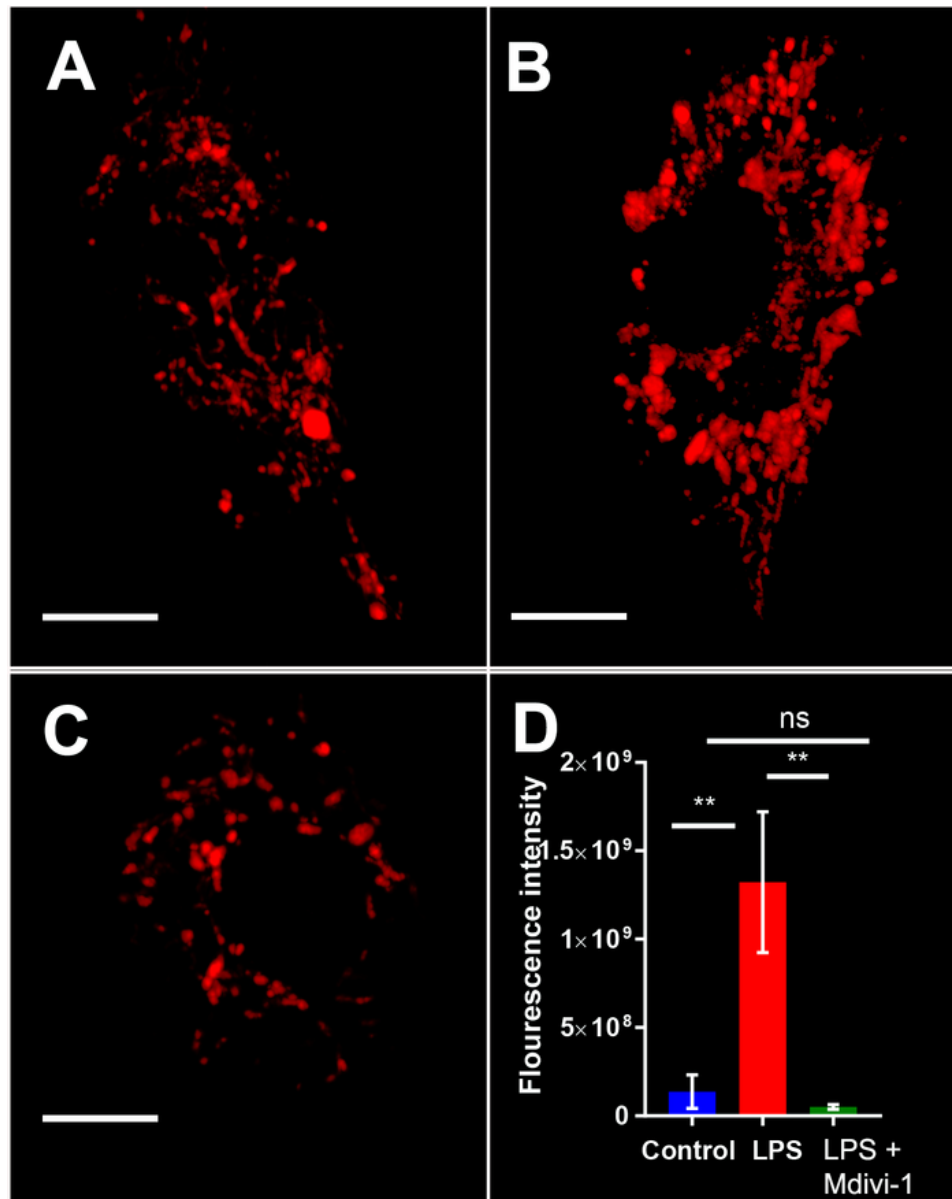


Fig.7 Mdivi-1 treatment abolished LPS induced mitochondrial ROS production. (A) Control (B) 100ng/ml LPS exposure for 24hrs (C) LPS+Mdivi-1 (D) Graphs showing results from an analysis of mitosox fluorescence by live cell airyscan microscopy. The data are for at least 12 cells per condition in three independent experiments. Bar graphs expressed as mean  $\pm$  SEM. \*\* $P \leq 0.01$ , student-t test calculating the difference between control LPS and Mdivi-1 treated groups.

59x74mm (300 x 300 DPI)

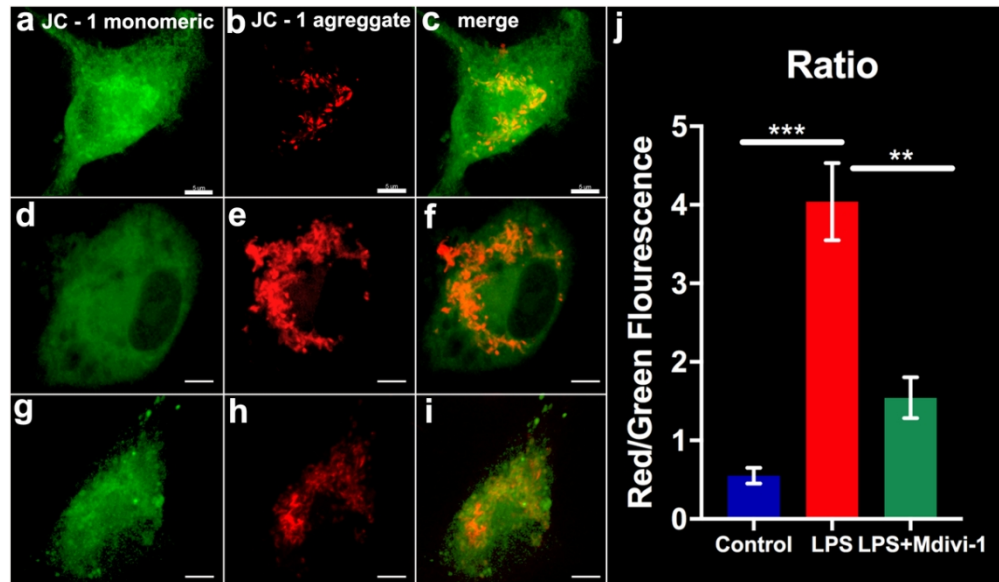


Fig.8 Mdivi-1 treatment attenuated LPS induced increase of mitochondrial membrane potential: (a-c) Control (d-e) 100ng/ml LPS exposure for 24hrs (g-h) LPS+Mdivi-1. Graphs showing results from an analysis of JC1 fluorescence 525/565 nm by live cell airyscan microscopy. The data are for at least 6 cells per condition in three independent experiments. Bar graphs expressed as mean  $\pm$  SEM. \*\* $P \leq 0.01$ , \*\*\* $P \leq 0.001$ , student-t test.

103x60mm (300 x 300 DPI)

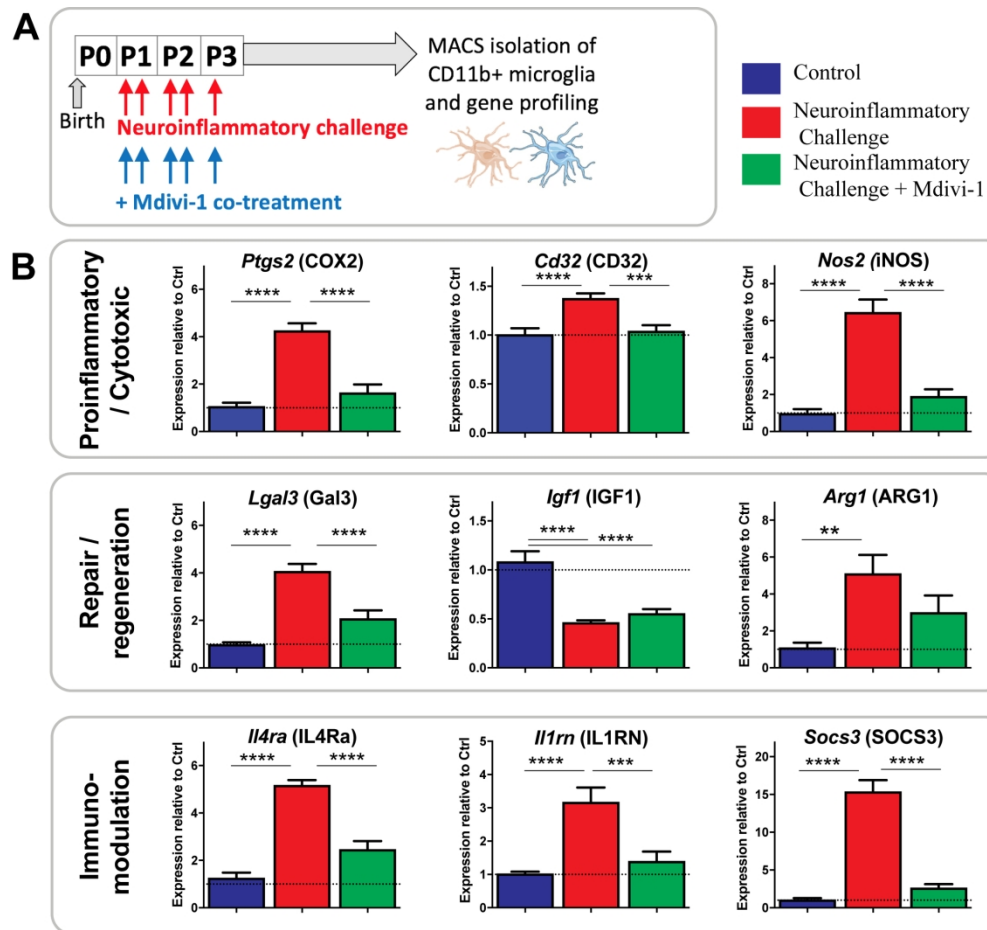


Fig.9 (A) Schematic representation of the testing of the effects of Mdivi-1 on neuroinflammation induced microglial gene expression in vivo. (B) Mdivi-1 prevented many of the neuroinflammation (IL-1 $\beta$ -induced) alterations in gene expression. Relative gene expression of *Ptgs2*, *Cd32*, *Nos2*, *Lgal3*, *Igf1*, *Arg1*, *Il4ra*, *Il1m* and *Socs3* were assessed by qRT-PCR from MACS isolated CD11b+ microglia from P3 mice. Protein names for the genes are shown in brackets on the panels. The legend indicates that the first bar (blue) is the control (PBS injected group), the middle bar (red) is the neuroinflammatory challenge group, and that the right bar (green) is the group challenged with neuroinflammation but also treated with Mdivi-1. The dotted line highlights the gene expression in the control group. Results are expressed as the mean  $\pm$  SEM. There are 10-15 data points from three independent experiments per group. Data were analysed with a Kruskal-Wallis ANOVA,  $P < 0.001$  with a Dunn's test for comparison among groups: \*\* $p < 0.01$ , \*\*\*  $p < 0.001$ , \*\*\*\*  $p < 0.0001$ .

190x177mm (300 x 300 DPI)

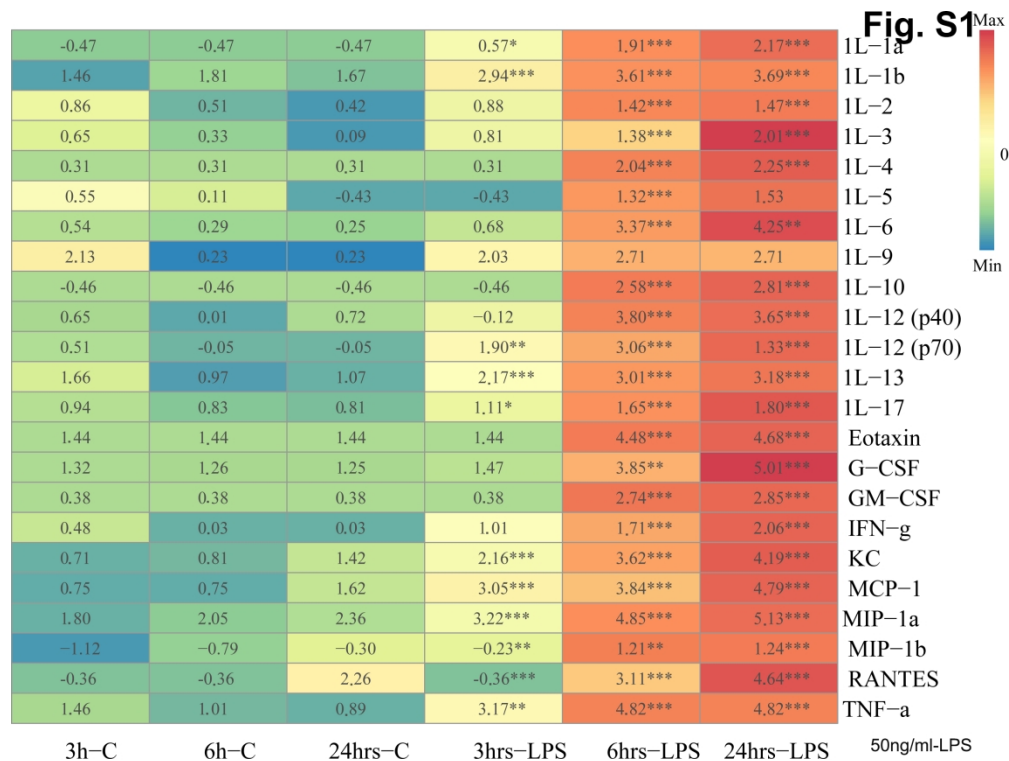
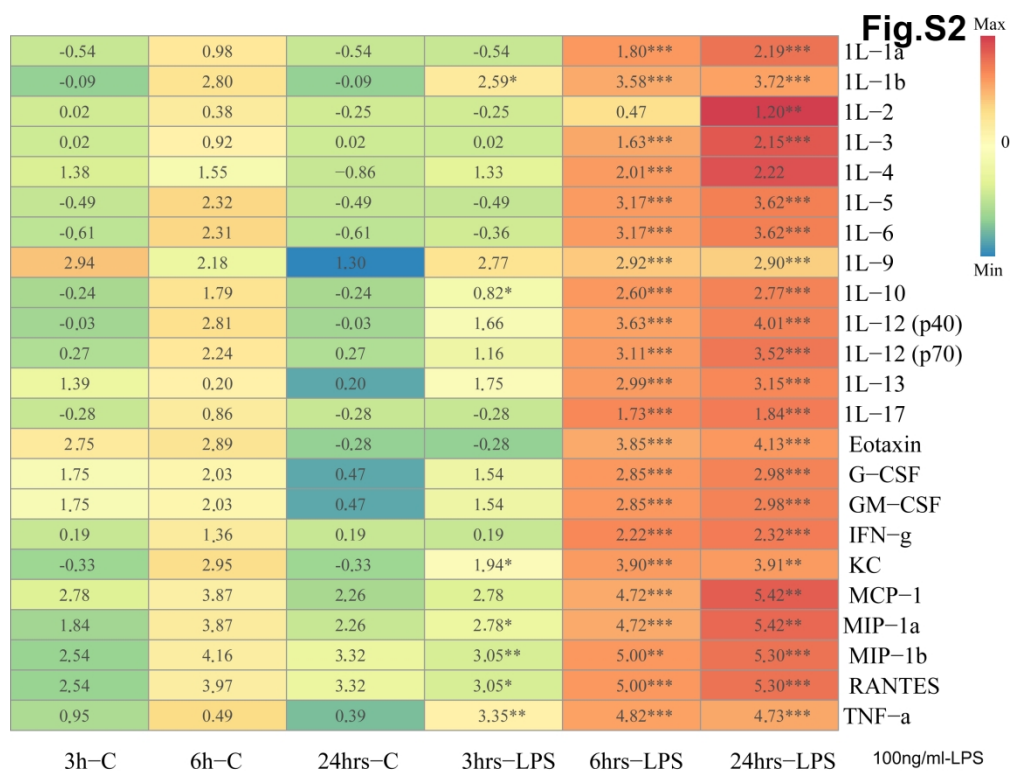


Fig. S1 and S2 (Supplementary) LPS induces exaggerated cytokine, chemokine following LPS exposure. The medium of microglial cells exposed with LPS 50 and 100ng/ml were sampled after 3,6 and 24h of LPS exposure and analyzed by 23-plex cytokine assay. Heat maps show the Log<sub>10</sub> of cytokine concentration (pg/ml). n=8 KC = keratinocyte chemoattractant. \*P ≤ 0.05; \*\*P ≤ 0.01; \*\*\*P ≤ 0.001; student-t test calculating the difference between control and LPS treated groups.



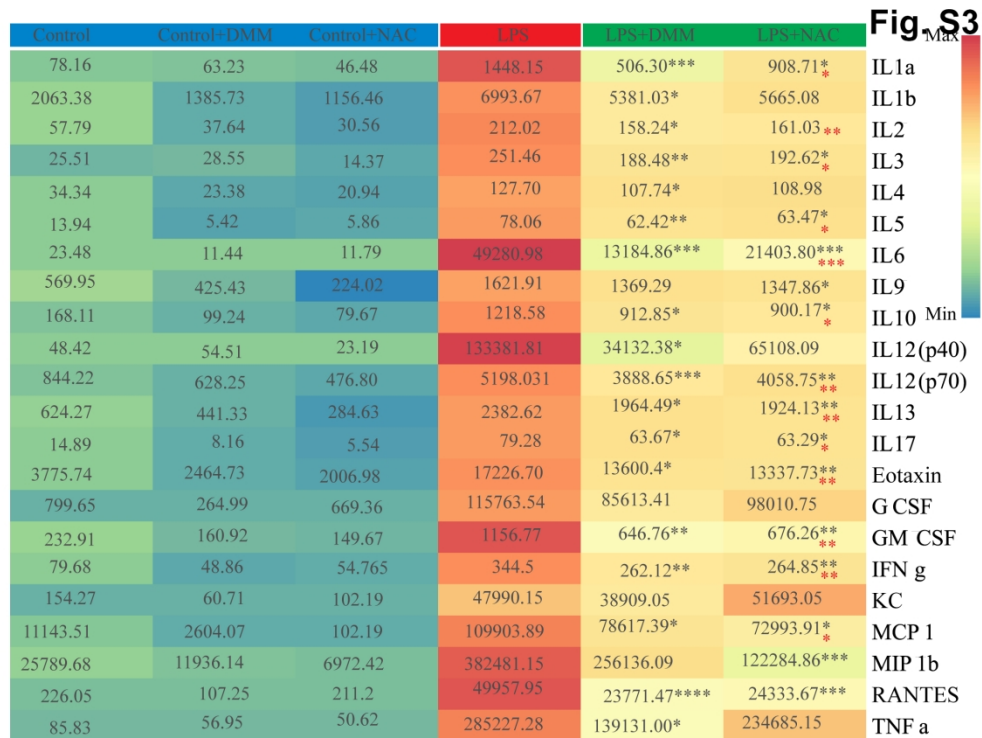


Fig.S3 (Supplementary) DMM or NAC attenuated LPS induces cytokine and chemokine production. Microglia cells were pre-treated with DMM (10mM, 3h) or NAC (10mM, 30 min) followed by LPS (100ng/ml) for 24hr, microglial culture medium was collected and analysed by 23-plex cytokine assay. Heat maps show cytokine concentration (pg/ml). KC = keratinocyte chemoattractant. n=8 \*P ≤ 0.05; \*\*P ≤ 0.01; \*\*\*P ≤ 0.001; One-way anova and turkeys multiple test calculating the difference between Control, LPS, LPS+Mdivi-1 and LPS+NAC treated groups. \*- rep significant difference with respect to LPS and treatment groups. \*- rep significant difference between treatment groups



**Supplementary Table 1: Primer sequences, protein targets and NCBI references**

<b>Gene</b>	<b>Target protein and abbreviation</b>	<b>Sense</b>	<b>Anti-sense</b>	<b>NCBI Reference</b>
<i>Inos</i>	Inducible nitric oxide synthase (iNOS)	CCC TTC AAT GGT TGG TAC	ACA TTG ATC TCC GTG ACA	NM_010927.3
<i>CD32</i>	Cluster of differentiation 32 (CD32)	CTG GAA GAA GCT GCC AAA	CCA ATG CCA AGG GAG ACT AA	NM_010187.2
<i>Ptgs2</i>	Cyclooxygenase-2 (Cox-2)	TCA TTC ACC AGA CAG ATT	AAG CGT TTG CGG TAC TCA TT	NM_011198.3
<i>Arg1</i>	Arginase-1 (Arg1)	GTG AAG AAC CCA CGG TCT	GCC AGA GAT GCT TCC AAC TG	NM_007482.3
<i>Lgals3</i>	Galectin-3 (Gal-3)	GAT CAC AAT CAT GGG CAC	ATT GAA GCG GGG GTT AAA GT	NM_010705.3
<i>Igf1</i>	Insulin like growth factor 1 (IGF-1)	TGG ATG CTC TTC AGT TCG	GCA ACA CTC ATC CAC AAT GC	NM_010512.4
<i>Il1rn</i>	Interleukin 1 receptor antagonist (IL-1Rn)	TTG TGC CAA GTC TGG AGA	TTC TCA GAG CGG ATG AAG GT	NM_031167.5
<i>Il4ra</i>	Interleukin 4 receptor alpha (IL-4R $\alpha$ )	GGA TAA GCA GAC CCG AAG	ACT CTG GAG AGA CTT GGT	NM_001008700.3
<i>Socs3</i>	Suppressor of cytokines 3 (SOCS3)	CGT TGA CAG TCT TCC GAC	TAT TCT GGG GGC GAG AAG AT	NM_007707.3